SLAC–PUB–6293
July 1993
(A)

A TEST ACCELERATOR FOR THE NEXT LINEAR COLLIDER[#1]

R. D. Ruth, C. Adolphsen, K. Bane, R. F. Boyce, D. L. Burke, R. Callin, G. Caryotakis, R. Cassel, S. L. Clark, H. Deruyter, K. Fant, R. Fuller, S. Heifets, H. Hoag, R. Humphrey, S. Kheifets, R. Koontz, N. M. Kroll,[#2] T. Lavine, G. A. Loew, A. Menegat, R. H. Miller, C. Nantista,[#3] J. M. Paterson, C. Pearson, R. Phillips, J. Rifkin, J. Spencer, S. Tantawi, K. A. Thompson, A. Vlieks, V. Vylet, J. W. Wang, P. B. Wilson, A. Yeremian, B. Youngman

Stanford Linear Accelerator Center,
Stanford University, Stanford, CA 94039, USA

Abstract

At SLAC, we are pursuing the design of a Next Linear Collider (NLC) which would begin with a center-of-mass energy of 0.5 TeV, and be upgradable to at least 1.0 TeV. To achieve this high energy, we have been working on the development of a high-gradient 11.4-GHz (X-band) linear accelerator for the main linac of the collider. In this paper, we present the design of a "Next Linear Collider Test Accelerator" (NLCTA). The goal of the NLCTA is to incorporate the new technologies of X-band accelerator structures, RF pulse compression systems and klystrons into a short linac which will then be a test bed for beam dynamics issues related to high-gradient acceleration.

#1 Work supported by the Department of Energy, contract DE–AC03–76SF00515.
#2 And at University of California, San Diego.
#3 University of California, Los Angeles.

Invited talk presented at the ECFA Workshop on e^+e^- Linear Colliders (LC92)
Garmisch-Partenkirchen, Germany, July 25–August 2, 1992

1. Introduction

To meet high energy physics requirements, the Next Linear Collider (NLC) should have an initial center-of-mass energy of 0.5 TeV (five times the SLC) with the capability of being upgraded to 1 TeV. This increase in energy can be obtained either by greatly increasing the length of the collider (by a factor of 10 to 20) relative to the SLC, or by increasing both the accelerating field and the length to obtain the desired energy. The present consensus at SLAC[1,2] is that we should first increase the accelerating field by about a factor of three to six—to about 50 to 100 MV/m. To limit the rf power required, this field would be provided by structures similar to those used in the SLC, but at the higher rf frequency of 11.4 GHz.

The luminosity required for high energy physics is about 10^{33}cm^{-2} sec^{-1} at the lower energy and about 4 times higher at 1 TeV. In principle, one could increase the luminosity simply by raising the repetition rate of the accelerator, but the wall-plug power would increase in direct proportion. In the NLC design at SLAC, we have limited the wall-plug power to about 250 MW. Given this constraint, the primary method to increase the luminosity is to shrink the beam size at the collision point. In addition, the beam cross section must be kept flat at the collision point in order to minimize the amount of "beamstrahlung" radiation and to control other beam-beam effects and backgrounds.

The luminosity can be further enhanced by accelerating several bunches within each machine pulse. A single bunch of particles can, in practice, extract only a few percent of the energy available in the accelerating structure. With additional bunches, both a greater luminosity and a higher efficiency of energy transfer to the beam are achieved. The number of particles in each bunch, another factor that directly affects the luminosity, is limited by the single-bunch beam loading in the accelerating structures, and by the amount of beamstrahlung radiation that can be tolerated at the final focus. Taking these effects into account, we accelerate a train of bunches, each with a fairly moderate number of particles, on each rf pulse.

Our working layout for the NLC is shown in Figure 1. The basic features of this layout are similar to other designs around the world and are based on extensive experience with the SLC. The working parameter set for the NLC is shown in Table 1. The parameters are not finalized, but the range of variation has narrowed considerably over the past few years.[1–5]

The primary parameter change recently has been an increase of the number of bunches accelerated on each cycle of the machine. This was caused by the desire to provide about an order of magnitude of overhead in the design luminosity for the NLC, couped with an increased understanding of multibunch instabilities and loading. With the overhead in design luminosity, the NLC can achieve the target 10^{33}cm^{-2} sec^{-1} with enhanced spot size or lower repetition rate or reduced number bunches. The increased number of bunches has led to an increased efficiency of energy transfer from the wall plug to the beam. The parameters shown for the 500 GeV version have an rf

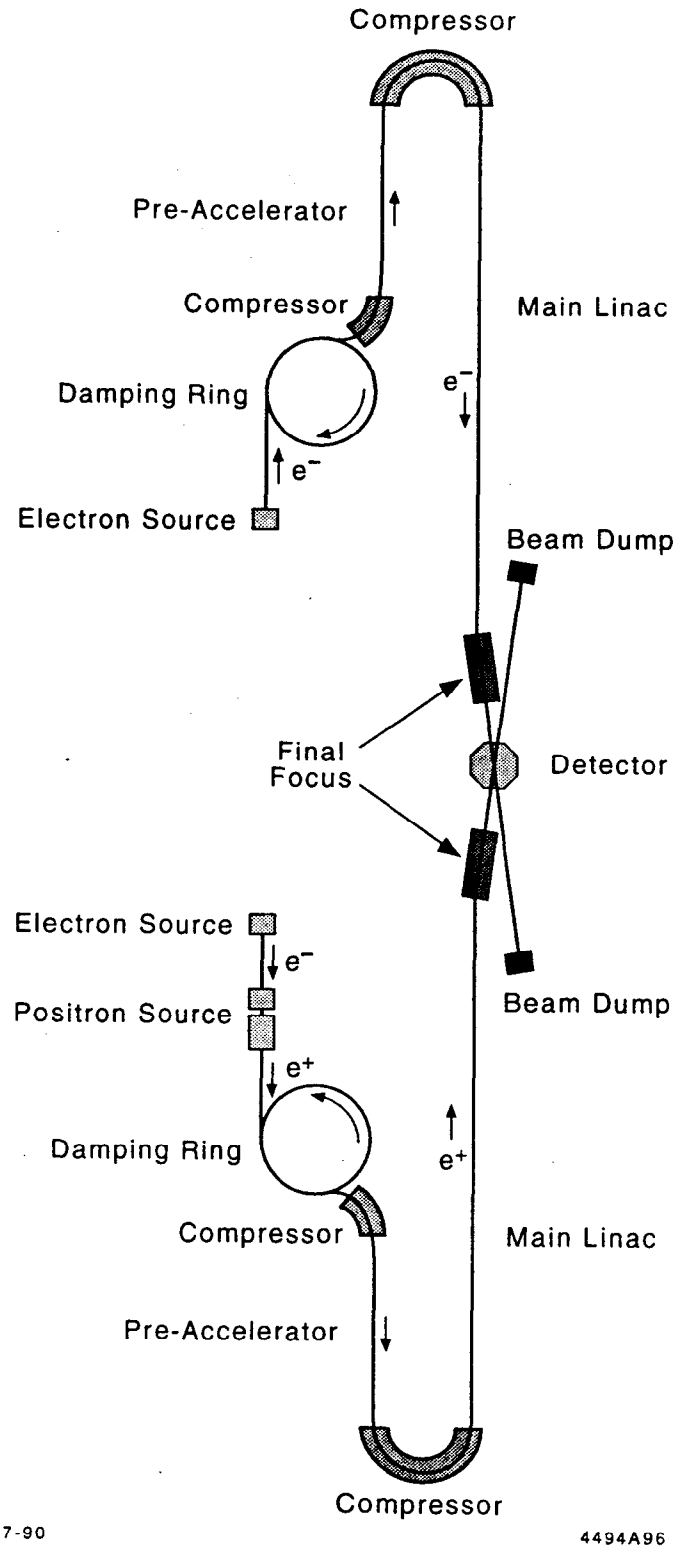

Figure 1. Possible layout of the Next Linear Collider.

Table 1. NLC Working Parameters

Parameter	500 GeV CM Energy	1 TeV CM Energy	Comments
E	250 GeV	500 GeV	Beam Energy
L_H	9×10^{33}	2.0×10^{34}	w/ Enhancement
$2\,L_{Linac}$	15 km	15 km	Total X-Band Linac Length
E_Z	50 MV/m	100 MV/m	Accelerating Gradient
f_{rf}	11.4 GHz	11.4 GHz	RF Frequency
N	0.65×10^{10}	1.3×10^{10}	Particles/Bunch
n_B	90	67	Number of Bunches
s_B	1.4 ns	1.4 ns	Bunch Spacing
f	180 Hz	120 Hz	Bunch Trains/sec
P_{beam}	4 MW	8 MW	Avg. Beam Power at IP
P_{wall}	160 MW	250 MW	Modulator Wall-Plug Power for Both Linacs
σ_x	300 nm	425 nm	variable
σ_y	3 nm	2 nm	$\gamma^{1/2}$ scaling
σ_z	100 μ	100 μ	Bunch Length
δ_{RMS}	2×10^{-3}	2×10^{-3}	Energy Spread

system efficiency (discussed in Section 2.2) of 19% while those for the 1 TeV upgrade include an improved efficiency of 27%. With the increased number of bunches, we obtain a wall plug-to-beam efficiency of 2.5% at 500 GeV and 3.2% at 1 TeV. The intensity of the single bunches has been limited to yield rather weak single bunch wakefield effects, comparable to the chromatic effects due to the normal focusing magnets. Finally, we consider it crucial to have a well-defined path to upgrade the energy (with increased luminosity) to the 1 TeV level. This is reflected in the 1 TeV design in Table 1 which is obtained with the addition of power sources to the main

linac.

The above considerations have led us to pursue a design based on warm rf linacs with unloaded gradients of 50 MV/m, upgradable to 100 MV/m at the rf frequency of 11.4 GHz.

During the past several years much experience has been gained with this rf frequency at SLAC and KEK. We have powered 11.4-GHz structures to reach peak surface fields in excess of 500 MV/m, and have achieved an accelerating gradient of 100 MV/m stably, for an extended period of time, in a 30-cell structure. High-power klystrons have been constructed which produce 50-MW pulses of 1-μs duration. We have constructed high-power rf pulse-compression systems which achieve a factor of five in peak-power multiplication. Designs for more efficient modulators have recently been completed and tests are under construction. Finally, we have developed low-loss microwave components for manipulating and transmitting 11.4-GHz high-power pulses.

Many of the outstanding questions related to achieving the NLC luminosity can be answered using the SLAC Final Focus Test Beam, the KEK ATF damping ring, and with dedicated experiments at the SLC. However, the details of the trade-off between linac length and accelerating gradient cannot be evaluated until a test has been made of a complete 11.4-GHz accelerating system. The primary missing ingredient for completing the NLC rf-system design is a test accelerator based on 11.4-GHz technology and designed specifically to study the range of parameters of interest for the NLC.[6] This brings us to the subject of this paper, the Next Linear Collider Test Accelerator (NLCTA).

One goal of the Next Linear Collider Test Accelerator (NLCTA) is to construct and operate reliably a high-gradient X-band linac in order to integrate the new technologies of X-band accelerator structures and rf systems being developed for the NLC. The NLCTA will serve as a test bed as the design of the NLC evolves, and will provide a model upon which a reliable cost estimate for an NLC linac can be based.

Other goals are to measure the growth of the accelerated "dark current" generated by rf field emission in full-length accelerator sections, to demonstrate multi-bunch beam-loading energy compensation at the 0.1% level for 25% steady-state loading, to observe the suppression of the higher-order deflecting modes of the accelerator structure, and to measure any transverse components of the accelerating field. In general, we will study the dynamics of the beam during the high-gradient acceleration of many bunches on each rf pulse of the X-band linac.

In the remainder of this paper, we discuss in detail the design of the NLCTA and conclude with discussion of some of the experiments that we wish to perform after completion.

2. Design of the NLC Test Accelerator

2.1. Overview

The Next Linear Collider Test Accelerator (NLCTA) will be a 42-meter-long beam line consisting, consecutively, of an injector, a chicane, a linac, and a spectrometer.

The injector will consist of a 150-kV gridded thermionic-cathode gun, an X-band prebuncher, a capture section, and a preacceleration section. Downstream from the injector will be a magnetic chicane for longitudinal phase-space manipulation. After energy collimation, the average current injected into the linac will be comparable to the NLC specification, $0.65 \times 10^{10} e/(1.4\,\mathrm{ns})$.

The NLCTA linac will consist of six 1.8-meter-long X-band accelerator sections which are detuned for higher-order-mode wakefield suppression. These sections will be powered by three 50-MW klystrons whose peak power will be quadrupled by SLED-II rf pulse compressors. This will yield an unloaded acceleration gradient of 50 MV/m so that the maximum energy gain of the beam in the X-band linac will be 540 MeV. The NLCTA rf system parameters are listed in Table 2.

Downstream from the linac will be a magnetic spectrometer that will analyze the bunch train after acceleration. A vertical kicker magnet in the spectrometer will provide a method for separating the bunches vertically so that the energy and energy spread may be measured along the bunch train. It will also be possible to measure emittance in the spectrometer and in the chicane.

We plan in the future to increase the linac gradient to 100 MV/m by replacing the three 50-MW klystrons that initially will power the linac with six 100-MW klystrons, as indicated in Table 2.

We also plan to upgrade the injector in order to increase the bunch spacing and intensity, each by a factor of 16. This will permit more detailed beam-dynamics studies on a train of bunches similar to that required for the NLC.

Views of the NLCTA are shown in Figures 2 through 6. The NLCTA will be located in End Station B (ESB) in a configuration that allows access to the overhead crane from the sliding concrete door on the south wall, and that retains the option to use existing Beam Lines 19 and 20 for future test beams if desired. The NLCTA will be contained in a six-foot-thick concrete shielding enclosure to be constructed inside ESB. The modulators, klystrons, and power supplies will be located next to this enclosure, inside ESB, in order to allow access to them while the NLCTA is running. The control room will be located outside, adjacent to the south wall of ESB.

Table 2. NLCTA RF System Parameters

Parameter	NLCTA Design	Energy Upgrade
Linac unloaded energy gain	540 MeV	1080 MeV
Linac active length	10.8 m	10.8 m
Unloaded accelerating gradient	50 MV/m	100 MV/m
Injection energy	90 MeV	90 MeV
RF frequency	11.424 GHz	11.424 GHz
Number of klystrons	3	6
Klystron peak power	50 MW	100 MW
Klystron pulse length	1.5 μs	1.5 μs
RF pulse compression power gain	4.0	4.0
Phase advance per cell	$2\pi/3$	$2\pi/3$
HOM suppression technique	Detuning	Detuning

2.2. RF System, Pulse Compression and Power Transmission

The high-gradient accelerator structure will be fed with rf power through overmoded circular waveguides which penetrate the shielding blocks above the accelerator. Four 50-MW klystrons will be positioned along the accelerator, outside the shielded enclosure. One of the klystrons will power the capture and preacceleration sections of the injector. The other three klystrons will power the six-section linac. Each klystron will be pulsed by an independent modulator. This will allow flexibility for multi-bunch energy control. It also will allow adequate modulator power for a future energy upgrade in which the three 50-MW linac klystrons are replaced by six 100-MW klystrons in order to achieve a 100-MV/m linac gradient, as indicated in Table 2. Each klystron will feed a SLED-II rf pulse compressor. The pairs of delay lines of the SLED-II pulse compressors will extend parallel to the accelerator, overlapped with one another, outside the shielded accelerator vault. The output of each SLED-II pulse compressor will be in overmoded circular waveguide that will enter the shielded vault through a penetration in a roof block. Inside the shielded vault, a mode transducer will split the power from the overmoded circular guide into two short rectangular waveguides, each of which will feed one accelerator section. The layout of the accelerator, klystrons, SLED-II pulse compressors, and waveguides is shown in Figures 2 through 6.

In the rest of this section, the overall performance of the NLCTA rf system is

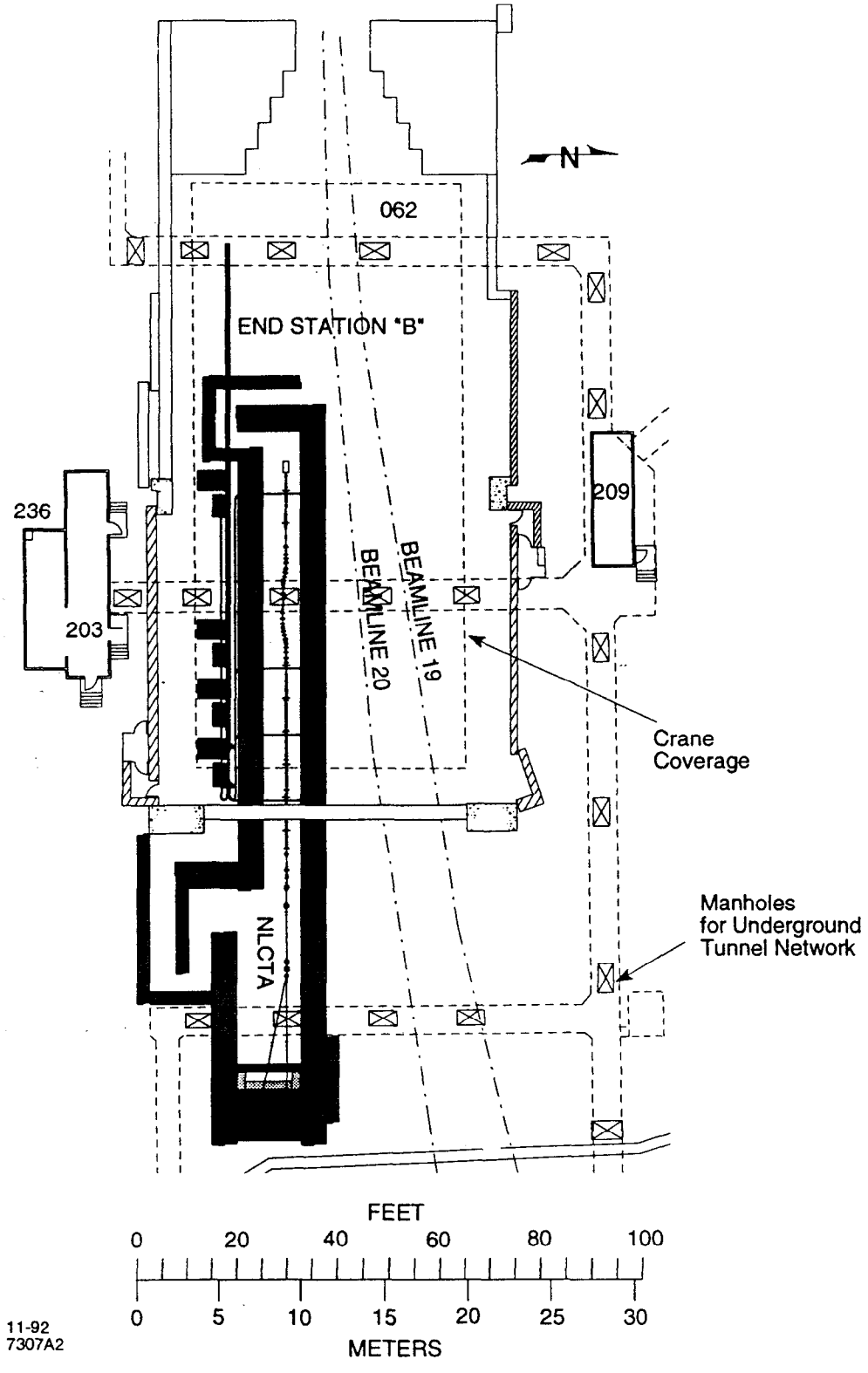

Figure 2. Plan view of the NLCTA site. New installations for the NLCTA (shielding, klystrons, modulators, beamline) are shaded. Electronics racks are not shown.

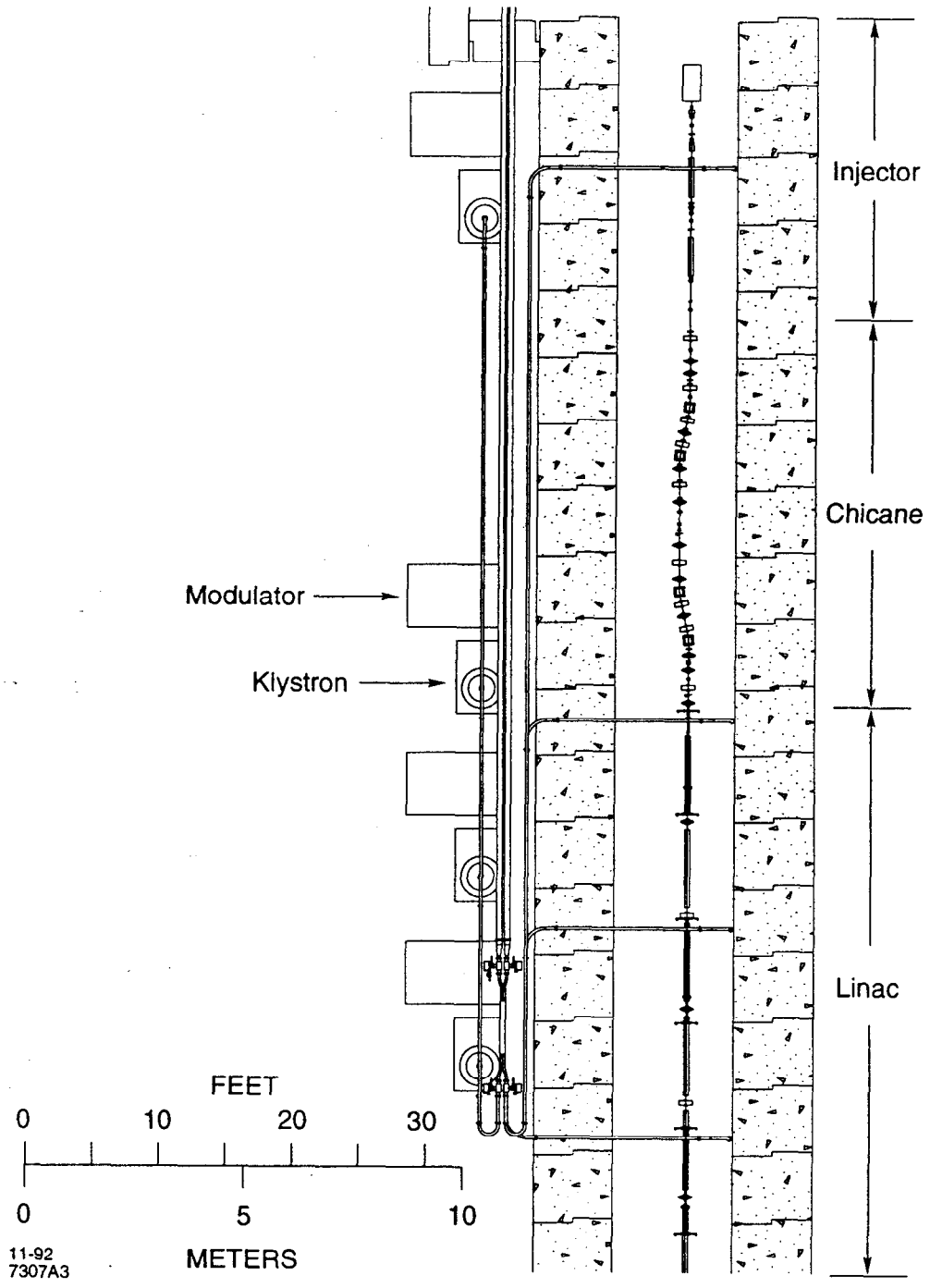

Figure 3. Plan view of the NLCTA injector, chicane, and linac.

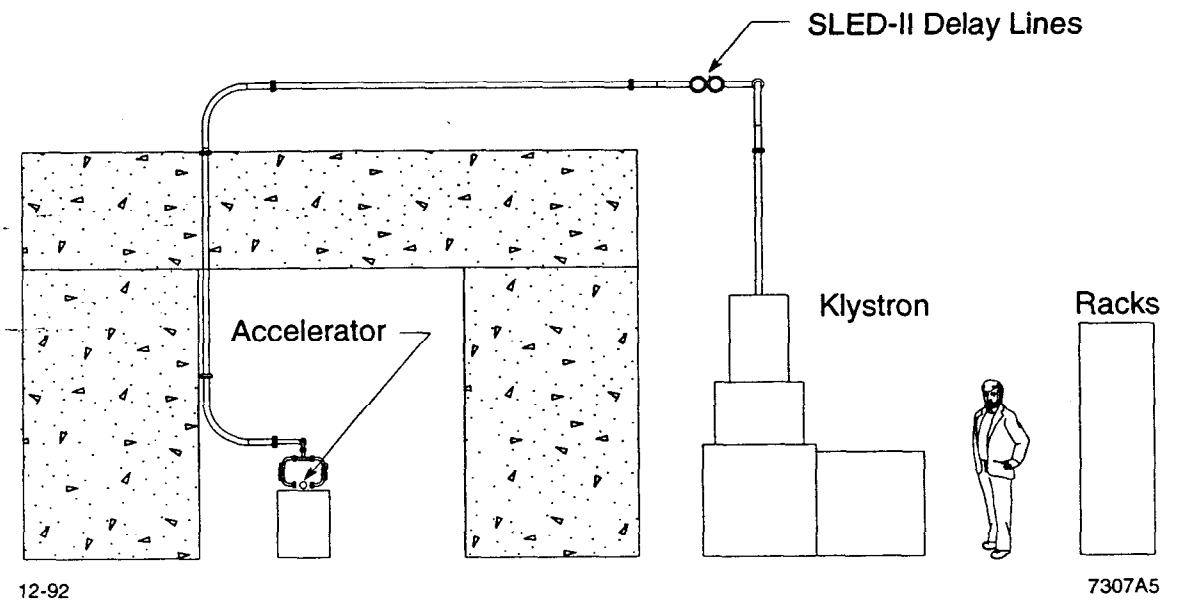

Figure 4. Cross-sectional view of the NLCTA linac.

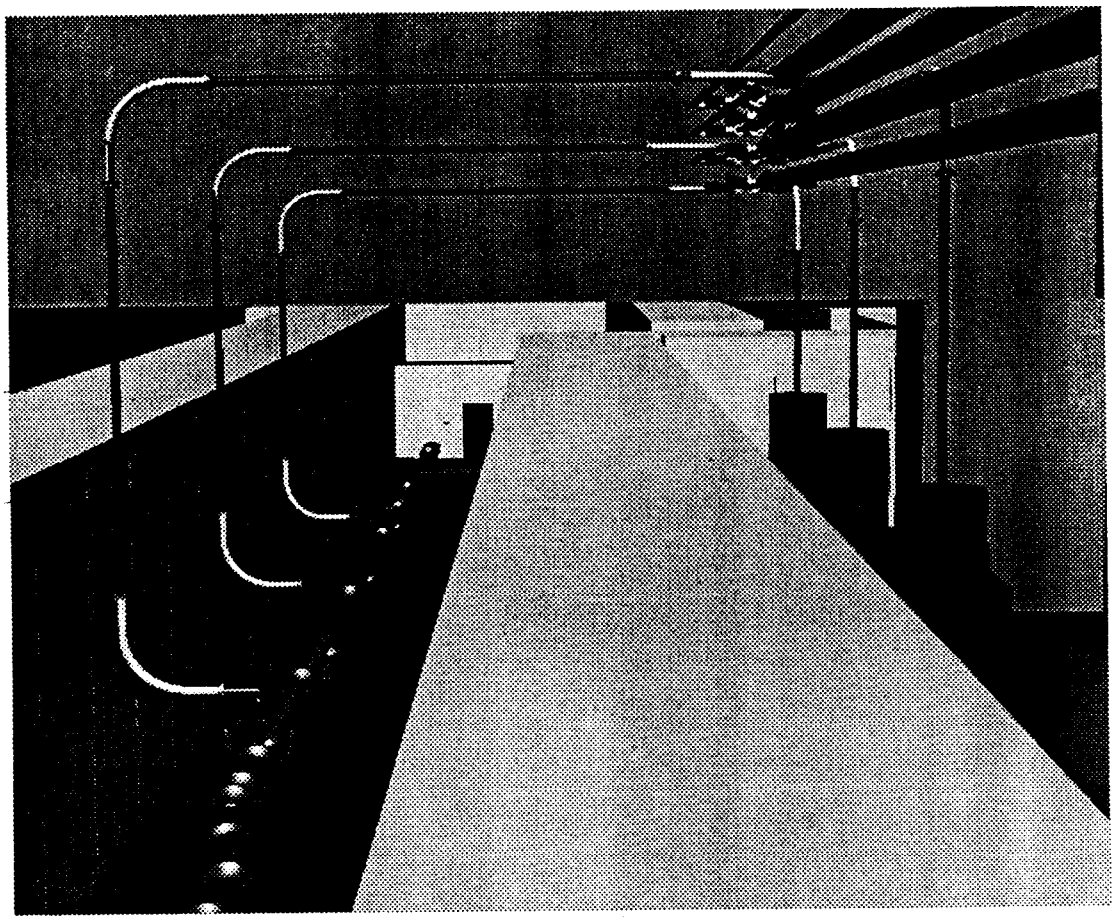

Figure 5. View looking down the NLCTA linac with the roof shielding removed. The beam line is visible to the left of the shielding wall. The klystrons and modulators are visible to the right.

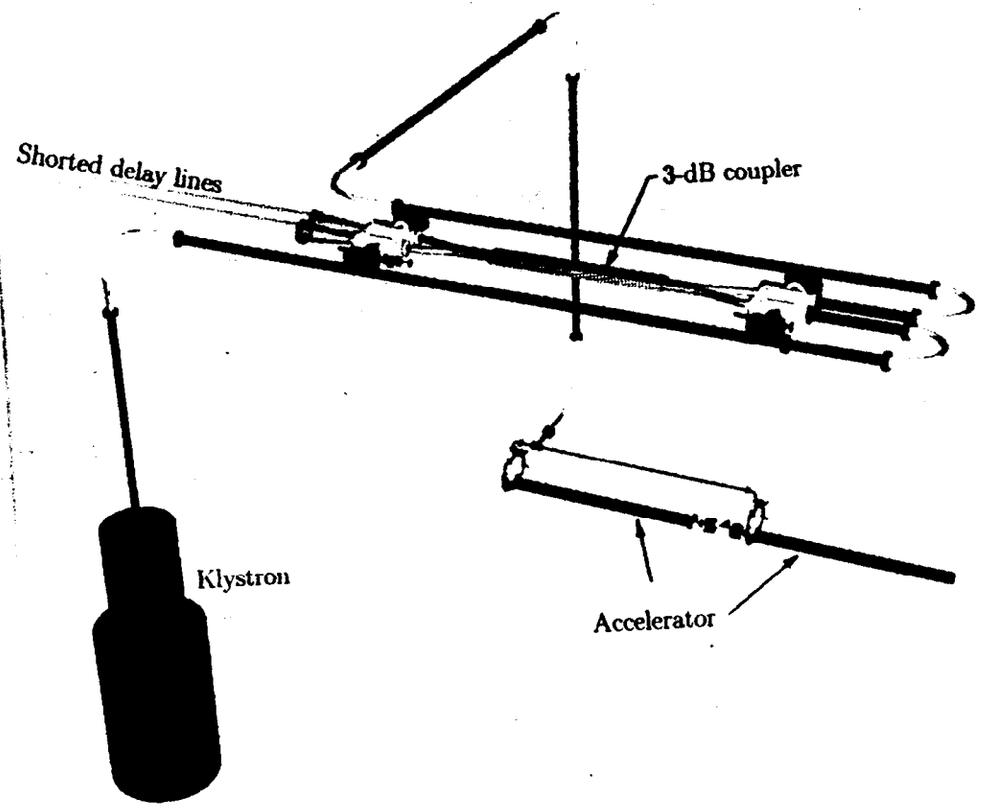

Figure 6. Layout of one NLCTA rf station consisting of klystron, SLED-II pulse compressor, and two accelerator sections. (The accelerator shielding is not shown.)

described, including klystrons, modulators, rf pulse compression, and rf power transmission. Details of the klystrons and modulators can be found in Sections 2.3 and 2.4.

A peak power of about 200 MW will be required to drive two 1.8-m-long sections of the accelerator structure (described in Section 2.5) to an accelerating gradient of 50 MV/m. A 250-ns rf pulse length at the accelerator input will provide 100 ns for filling the structure, 125 ns for accelerating the bunch train, and 25 ns for rise- and fall-times. In Table 3, the peak power and energy per pulse are tracked backward through the rf system, starting at the accelerator feeds, for accelerating gradients of 50 MV/m and 100 MV/m. Power will be transmitted from the output of the SLED-II rf pulse-compressor to the feeds of the accelerating structures with an efficiency of about 88%. This estimate is based on theoretical calculations and measurements of prototypes. The losses of the individual components of the power-transmission system will be: 1% for 10 meters of 3-inch-diameter circular waveguide, 2% each for three 90° circular waveguide bends, 2% for one power-splitting mode transducer, and 3% for the rectangular waveguide feeds to the accelerator. There will be an additional 2% loss in transmitting power from the klystron output to the input of the SLED-II pulse compressor (assuming one 90° bend), giving a net power transmission efficiency of about 86% from klystron to accelerator.

A SLED-II rf pulse compressor[7,8,9] will compress the 50-MW, 1.5-μs-long klystron pulse by a factor of six in time to 250 ns and, in doing so, will multiply the peak power by a factor of 4.0, to 200 MW, with a compression efficiency of 67%. As shown in Figure 6, the main components of the SLED-II rf pulse compressor are a 3-dB coupler (power divider) and two shorted, 36-m-long, 4.75-inch-diameter, circular-waveguide delay lines. The down-and-back transit time of each delay line is equal to the required compressed pulse length of 250 ns. The delay lines operate overmoded in the TE_{01} mode in order to reduce power losses. The pulse length of the SLED-II input pulse (klystron output pulse) can be any multiple of 250 ns. A larger compression factor gives a higher power gain, at the expense of reduced compression efficiency.

SLED-II pulse compressors have an intrinsic inefficiency in addition to any inefficiencies due to component losses. The intrinsic inefficiency is the result of energy incident on the delay lines being reflected from the delay line entrance aperture (an iris) prior to the formation of the high-peak-power SLED-II output pulse. Also, a small amount of rf energy remains in the delay lines after the output pulse. For pulse-length compression by a factor of six, the intrinsic efficiency of SLED-II is 75%. (This is obtained with an iris-reflection coefficient of 0.685.) In addition, there is a 4% power loss in the 4.75-inch-diameter copper delay lines, and a 6% loss in the 3-dB coupler. This brings the net compression efficiency down to 67%, as shown in Table 3.

An important consideration in modulator performance is the efficiency for the transfer (through a pulse transformer) of energy stored in the capacitors of the pulse-forming network (PFN) to useful energy in the flat-top portion of the output pulse. This efficiency is given roughly by $T_p/(T_p+\alpha T_r)$, where T_p is the time duration of the flat-top, T_r is the pulse rise-time, and α is a coefficient of order one. In turn, the rise-

Table 3. NLCTA RF System Performance

	NLCTA Design	Energy Upgrade
Accelerator Structure		
Gradient (MV/m)	50	100
Pulse length (ns)	250	250
Peak power per feed (MW)	87	350
Pulse energy per feed (J)	22	87
Feeds per klystron	2	1
Power Transmission Efficiency	0.86	0.86
Pulse Compression		
Peak output power (MW)	200	800
Pulse energy (J)	50	200
Power gain	4.0	4.0
Compression ratio	6	6
Compression efficiency	0.67	0.67
Klystron		
Peak output power (MW)	50	100
RF pulse length (μs)	1.5	1.5
Klystron efficiency	0.45	0.45
Modulator		
Klystrons per modulator	1	2
Peak output power (MW)	110	440
Modulator efficiency	0.73	0.73
PFN stored energy (J)	220	870
AC input power (kW) at 180 pps	41	165
RF System Net Efficiency	0.19	0.19

time is roughly proportional to the turns-ratio of the pulse transformer. In the present modulator design (see Section 2.4), the transformer turns ratio is reduced by using a three-stage "multiplying Blumlein" design for the PFN. This allows a factor-of-three reduction in the transformer turns-ratio from about 20:1 to 6:1, a corresponding decrease in rise-time, and an increase in energy-transfer efficiency to about 77%. The overall modulator efficiency quoted in Table 3 is 73%, because of the fact that there is an additional 5% loss in the front-end modulator components (such as the dc power supply, transformers, charging choke, *etc.*). Finally, it should be noted that, although the use of an rf pulse-compression system introduces additional (intrinsic) losses, they are nearly compensated by the increase in modulator efficiency gained because of the longer klystron pulse length. Thus, the net efficiency of the rf pulse compressor and the modulator tends to remain at about 50%, nearly independent of pulse length.

The NLCTA rf system will in the future be upgraded to double the accelerating gradient to 100 MV/m. This would require klystrons (or other rf sources) producing about 200 MW (or pairs of sources, each producing 100 MW). A two-stage rf pulse-compression system is another possibility, which would reduce the power source requirement to about 120 MW per source (or 60 MW per source, if deployed in pairs).

Development and testing of the individual components required for the SLED-II system are underway. It is expected that high-power tests on a full SLED-II prototype will be completed early in 1993. A high-power binary pulse-compression system, which uses overmoded components similar to those required for the SLED-II systems, is presently in use, providing power to the Accelerator Structure Test Area in the Klystron Test Laboratory at SLAC. In the binary pulse compressor, rf pulses are compressed by a factor of eight, with a factor of five increase in peak power.[10] So far, the highest peak output power achieved in binary pulse compression is 160 MW in a 70-ns pulse. This peak power was limited by the maximum available klystron power at the time of the test, and not by the pulse-compression system itself.

Implications for the NLC

The rf system performance in Table 3 can be extrapolated to a full-scale NLC. Assume 25% beam-loading so that the loaded gradient is 37.5 MV/m. Then, the active structure length required for acceleration to 500 GeV is 14 km, assuming an additional 5% overhead due to off-crest operation, *etc.* The number of NLCTA units (3.6 meters of structure plus a power source) required would be 3890. At 180 pps, the total wall-plug power for the rf system would be about 160 MW. In this scenario, one modulator could easily feed two klystrons, so only 1945 modulators would be required. However, the energy stored in the pulse-forming network would double to 440 J, and the wall-plug power per modulator would double to 82 kW.

An increase in the rf system efficiency would be very desirable. At a more favorable compression ratio of 5:1, and with some reduction in component losses due to continuing research and development, the efficiency of the rf pulse-compression system could be increased to about 77%. Assuming that the modulator efficiency were improved slightly (from 73%) to 75%, that the power transmission efficiency were

increased (from 86%) to 92%, and that the klystron efficiency were increased (from 45%) to 50%, then the overall rf system efficiency would be increased (from 19%) to 27% and the wall-plug power for the above example would be reduced (from 160 MW) to 115 MW.

If the energy of the NLC were doubled to 500 GeV per beam by increasing the gradient to 100 MV/m, if the repetition rate were reduced to 120 pps, and if the number of bunches was reduced to 65 (reducing the rf pluse length at the accelerator to 200 ns), then the wall-plug power would be about 250 MW, again assuming that the above higher efficiencies had been achieved.

2.3. KLYSTRONS

In order to satisfy the rf power requirements of the NLCTA, a 50-MW X-band klystron is being developed[11,12] to operate at pulse lengths up to 1.5 μs. The operating parameters of this klystron are shown in Table 4. A reliable 50-MW tube is an interim goal of the ongoing development of a 100-MW klystron at SLAC. By March 1993, eight versions of the 100-MW klystron will have been tested, and the final design of the 50-MW interim tube for the NLCTA will have been chosen. Subsequent 100-MW-development work will follow the production and testing of the 50-MW klystrons for the NLCTA.

Table 4. 50-MW Klystron Design Parameters

Operating frequency	11.424 GHz
Peak output power	50 MW
RF pulse width	1.5μs
Pulse repetition rate	180 pps
RF pulse rise-time	$\leq$ 10 ns
Beam voltage	440 kV
Beam current	350 A
Beam-to-rf efficiency	45%
Saturation gain	55 dB
Focusing field	5 kG

The first eight experimental tubes are designated XC1 through XC8. At the time of this writing, testing of XC1 through XC5 has been completed, and testing of XC6 is in progress. The progress to date in power capability is shown in Figure 7.

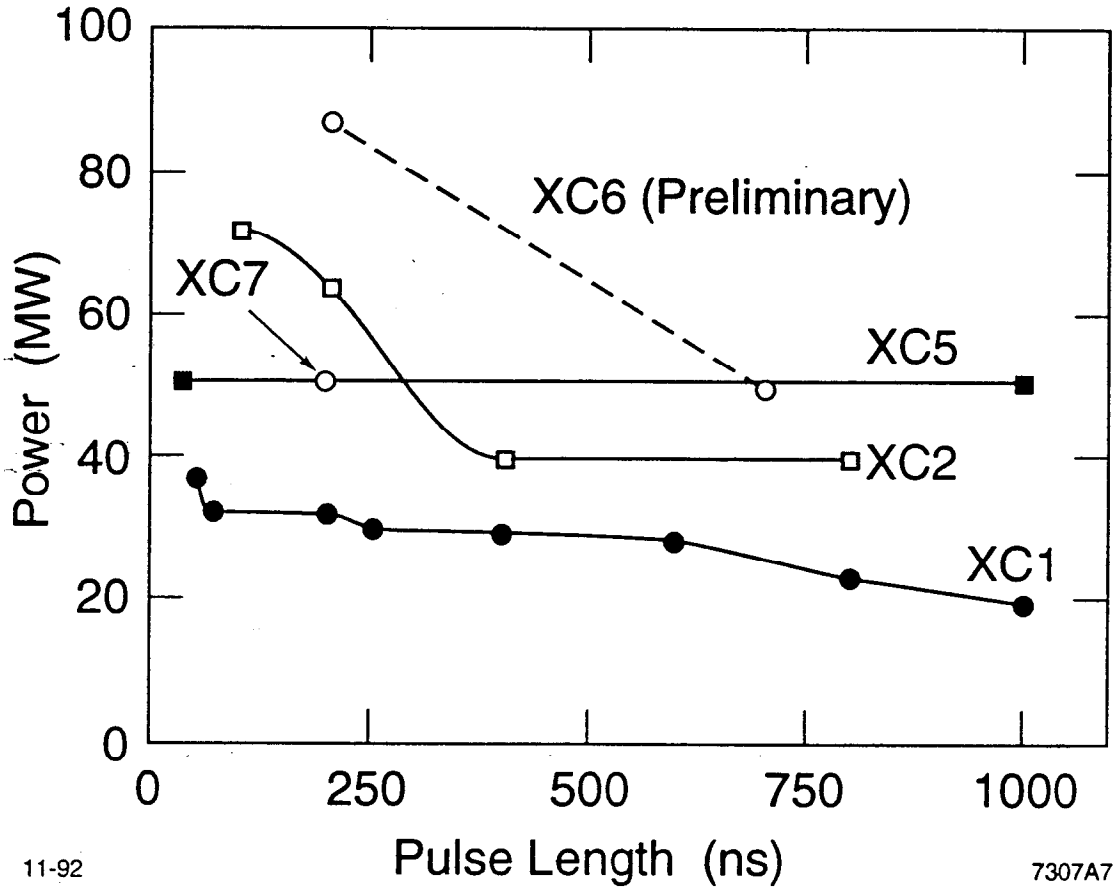

Figure 7. Power capability of the experimental X-band klystrons.

The first five tubes had in common the designs of their input, gain, and penultimate cavities. The output cavities of XC1 through XC4 included various arrangements of single-gap, and inductively coupled double-gap output cavities of the same beam-tunnel diameter as the input cavities. These first four tubes showed promise in terms of peak-power production at short pulse lengths, with a maximum of 72 MW. However, none was capable of 50 MW at pulse lengths of 1-μs or longer. Later inspection of XC1–XC4 showed severe damage to the output cavities.

The fourth klystron (XC4) included a new electron gun design which improved beam transmission. Failure to obtain an improvement in either performance or survivability ruled out beam quality as the primary cause of failure at long pulse lengths.

Based on the evidence, two modifications were made to the output circuit: (1) The beam-tunnel diameter was increased to better isolate the microwave circuit from the beam. (2) The symmetry of the output structure was improved to avoid field distortions which might steer the beam into the microwave circuit. To meet these conditions, XC5 incorporated a disk-loaded travelling-wave output section, with a 36% increase in beam-tunnel diameter and dual output waveguides for better output coupling symmetry. The performance of XC5 was a major improvement over earlier tubes in the series (see Figure 7). The 50-MW peak power achieved was similar to the previous tubes. However, XC5 operated successfully with 50 MW at 1-μs pulse length. The tube was opened after a subsequent heater failure and the disk-loaded output circuit showed some signs of overheating, indicating that further refinement of the design still was needed.

An additional weakness in the basic design of the early tubes was underscored by the results of the extensive testing of XC5. It had previously been recognized that the rf windows were marginal at the high peak power. The testing of XC5 was interrupted twice by window failures, which required replacement of the windows and reprocessing of the tube. Analysis of all window failures to date shows that the failures originated at the junction between the window and the waveguide, where the rf electric-field lines terminate. Consequently, a program was initiated to develop a TE_{01}-mode output window. This new window should be free of the previously observed failure mode because, in the TE_{01}-mode, no electric-field lines terminate at the braze junction between the window and the waveguide wall. Thus far in our TE_{01}-mode window development we have achieved 98% mode-purity and a good rf match in setting up the TE_{01} mode and transmitting it through the circular window. High-power tests of this new window design in a resonant ring are planned.

The final three tubes of the XC development series incorporate the following design modifications.

XC6 has gun and gain sections similar to XC3 and XC4. However, the output circuit consists of two uncoupled resonant cavities, each with two output waveguides, resulting in a total of four output windows. The elimination of the inductive coupling iris between the cavities lends to XC6 a symmetry not present in any of its four predecessors, as does the use of four symmetrical output waveguides. Dividing the

power among four output windows, though not a desirable long-term solution, allows us to obtain long-pulse, high-power operation with less concern for window failure. Preliminary results of testing XC6 are shown in Figure 7. The preliminary tests imply that the power capability of XC6 at shorter pulse lengths is at least as good as XC5. The power capability of XC6 at longer pulse lengths has not yet been explored.

XC7 will be identical to XC5, except for improvements to the disk-loaded travelling-wave output section which will contain four cavities instead of three for higher efficiency. The beam-tunnel diameter in the output section will be larger than in XC5 for greater isolation of the microwave circuit from the electron beam, and for lower surface-field gradients. The beam exit conditions have been altered by increasing the pole-piece diameter to overcome the melting of the collector which was observed in XC5.

XC8 incorporates a disk-loaded four-cavity resonant output circuit which features the lowest surface-field gradient of any of the circuits tested. The beam tunnel of the circuit is also larger in diameter than any of the previous circuits. In order to compensate for the adverse impact this might otherwise have on efficiency, the XC8 circuit includes an improved drive section, incorporating two additional cavities, which will provide the output circuit with 20% more rf current than that available in the earlier tubes. This tube will also include the new higher-power TE_{01} window that was discussed above.

A longer-term consideration in developing an economical NLC rf system is the power consumed by the solenoidal electromagnet which focuses the beam in each klystron. We have designed a periodic permanent-magnet (PPM) focusing system which could provide the necessary focusing without consuming power. The PPM focusing system will be tested in 1993. As a backup to the relatively high-risk PPM focusing development, the feasibility of using superconducting solenoids also is being investigated.

2.4. MODULATORS

The NLCTA 50-MW klystrons could in principle be driven by the same SLAC-type modulators now in use to power the X-band klystron test stands in the Klystron Test Laboratory. Parameters for the SLAC-type modulator, using a 20:1 turns ratio pulse transformer but having a longer pulse flat-top (1.5 μs *vs.* 0.9 μs), are shown in Table 5. However, this high pulse-transformer turns ratio leads to a large leakage inductance and hence to long pulse rise- and fall-times, implying a low modulator efficiency. The energy contained in the flat-top portion of the pulse applied to the klystron is only 58% of the energy stored in the capacitors of the pulse-forming network. This poor energy-transfer efficiency implies an excessive wall-plug power for a full-scale NLC.

A new modulator design has been proposed[13] that uses a multiplying Blumlein (or Darlington) pulse-forming network, which allows a reduction in the turns ratio of the pulse transformer to 6:1 for the same output pulse voltage. This leads to

Table 5. Modulator Parameters

SLAC-Type: Standard SLAC modulator with 20:1 Pulse Transformer.
Proposed: 1.5-times multiplying Blumlein PFN.

	SLAC-type	Proposed
Charging voltage (kV)	50	70
Pulse voltage (kV)	480	600
Pulse ±1% flat-top (μs)	1.5	1.5
Pulse rise-time to 99% (μs)	1.0	0.4
Pulse energy width (μs)	2.5	1.9
Energy-transfer efficiency	0.58	0.77
Net modulator efficiency	0.54	0.73

decreased rise-time and better energy-transfer efficiency, as indicated in Table 5. The output pulse shape for the proposed modulator design is compared with the present SLAC modulator pulse in Figure 8. The improved rise-time and a substantial gain in efficiency are evident from the figure. Conversion of a standard modulator in the Klystron Test Laboratory to the new design for testing is planned during FY93.

The conversion will involve rebuilding the modulator with a new Blumlein pulse-forming network and a new pulse transformer. The present thyratron and charging supply will be retained. While this design provides sufficient pulse voltage and current for the 50-MW X-band klystron, a pulse voltage on the order of 600 kV will be needed to produce power at the 100-MW level necessary for a 100-MV/m accelerating gradient. Table 5 lists the parameters for a proposed modulator using a thyratron and dc charging supply with a higher voltage capability, which increases the voltage on the pulse-forming network to 70 kV.

Note that in Table 5 the net modulator efficiency is lower than the energy-transfer efficiency referred to above. This difference is due to losses in the input transformers, dc power supply and the resonant charging circuit. This "front end" efficiency is taken to be 93% for the present modulator design and slightly higher for the proposed design.

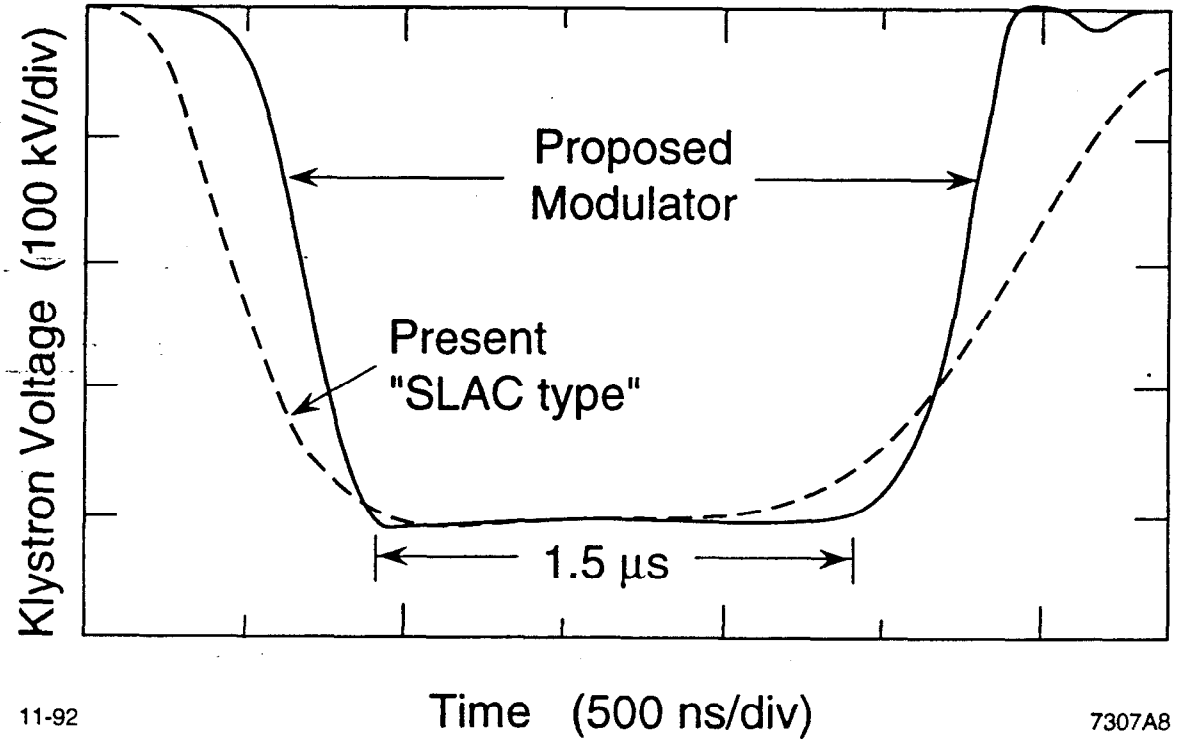

Figure 8. Comparison of a SLAC-type modulator (scope trace) with a simulation of the proposed modulator.

2.5. Accelerator Structure

The NLC design calls for accelerating a train of 90 bunches on each rf pulse in order to achieve the desired luminosity. One limitation of this approach comes from the coupling of the betatron motion of the bunches due to the long-range wakefields generated in the accelerator structures. If not controlled, these wakefields will produce a large growth in the transverse motion of the bunches which will lead to luminosity degradation and possibly beam breakup. To control this growth, the wakefields witnessed by the bunches must be reduced by about two orders of magnitude. Two methods are being considered to achieve this reduction, each of which has been tested experimentally.[14,15] In the first, the higher-order modes in the structure are damped by coupling them to radial waveguides which are terminated in matched loads. The second technique involves making the higher-order-mode (HOM) frequencies different for each cell while keeping the $\frac{2}{3}\pi$ phase shift in the accelerating mode constant. To the subsequent bunches following behind the driving bunch, the total wakefield, which is the sum of wakefields from the individual cells, decoheres because of the different frequencies of its components. Consequently, the effective wakefield is reduced.

For the NLCTA, we plan to use the detuned structure being developed at SLAC as a prototype for the NLC.[16] Parameters of this structure are listed in Table 6. Although the NLCTA initially will not have the NLC bunch spacing for which the structure detuning is designed, the wakefield supression still will be effective at preventing beam breakup.

The structure design uses a truncated Gaussian distribution of the HOM frequencies to produce a Gaussian fall-off in the initial time dependence of the wakefield. For this purpose, the relative distribution of HOM frequencies of the 204 cells in a section will have a standard deviation of 2.5% and will be truncated at $\pm 5\%$. This distribution can be obtained by modifying the design of a constant-gradient section so that the detuning is most pronounced for the cells near the ends of each section. This will result in a structure in which the iris sizes decrease rapidly at the beginning, decrease more slowly in the middle, and decrease rapidly again toward the end of each section.

Figure 9 shows a comparison of the accelerating field obtained for a square input rf pulse of 100-MW amplitude in three different cases: constant impedance, constant gradient, and Gaussian-detuned HOM.

With this distribution of HOMs, the wakefield will decohere to much less than 1% of its peak value early in the 40-meter-long bunch train, and then will recohere partially, as illustrated by Figure 10 which was obtained using an equivalent-circuit-model calculation[17] that incorporates cell-to-cell coupling.

Simulations of bunch transport in the NLC show that this decoherence is sufficient to control beam breakup if several sets of detuned accelerator sections with different sets of HOM frequencies, slightly displaced with respect to each other, are used. The implications for bunch transport in the NLCTA are discussed in Section 2.6.

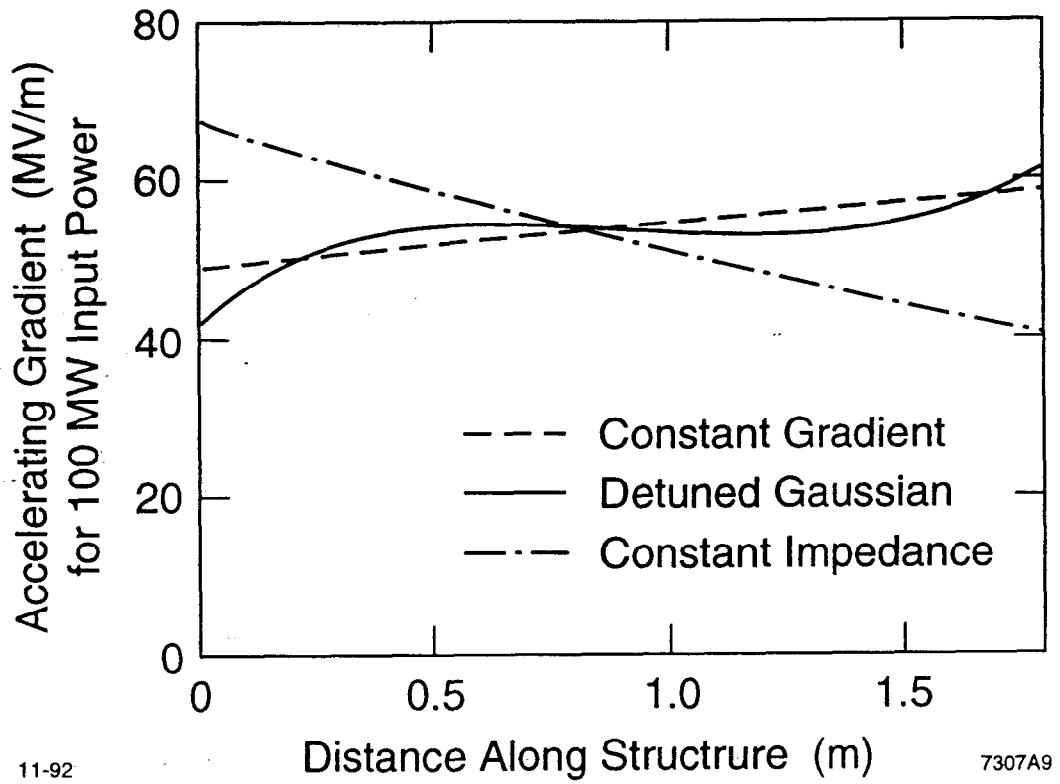

Figure 9. Comparison of accelerating field profiles in a 1.8-m-long accelerator section for 100-MW input power.

Table 6. NLCTA Structure Parameters

Section length	1.8 m
Phase advance per cell	$2\pi/3$
Iris aperture radius	5.72–3.91 mm
Iris aperture normalized radius	0.218λ–0.149λ
Group velocity	$0.12c$–$0.03c$
Filling time	100 ns
Unloaded time constant	207–186 ns
Attenuation parameter	0.517 nepers
Elastance ($\omega R/Q$ per unit length)	853–946 V/pC/m
Peak input power/(1.8 m) for 50 MV/m	48.1 MW/m
Peak power per feed for 50 MV/m	86.5 MW
Structure average power dissipation for 50 MV/m, 250-ns pulse length, 180 pps	1.4 kW/m

Mechanical Design of the Structure

Sketches of an NLCTA accelerator section and its individual cells are shown in Figures 11 and 12, respectively. Each cell of a section will have different cavity diameter, iris diameter, and iris wall thickness. All dimensions will be calculated to give the required dispersion characteristics for the fundamental mode and for the higher-order dipole modes, as described above.

Six cells (one close to each end, and four evenly distributed between them) will have radial pumping holes connecting the central (beam) cavity to two outer vacuum manifolds. These manifolds will each be connected to two 8-liter/s vacuum pumps in the middle of the section. The manifolds will increase the pumping speed through the small beam apertures by an order of magnitude. This improvement is considered necessary to handle the increased gas load resulting from high peak power rf propagating through the structure.

Four water-cooling tubes will be brazed along the outside of each section, as shown in Figure 11. The outer surface of each cell can be used for precise support and alignment since it is concentric to the iris diameter to within a few microns. Two tuning stubs will be brazed into each cell wall to permit fine tuning of the phase advance per cell of a completed section. Symmetrical double-input couplers will be used at the ends of each section to minimize the phase and amplitude asymmetries

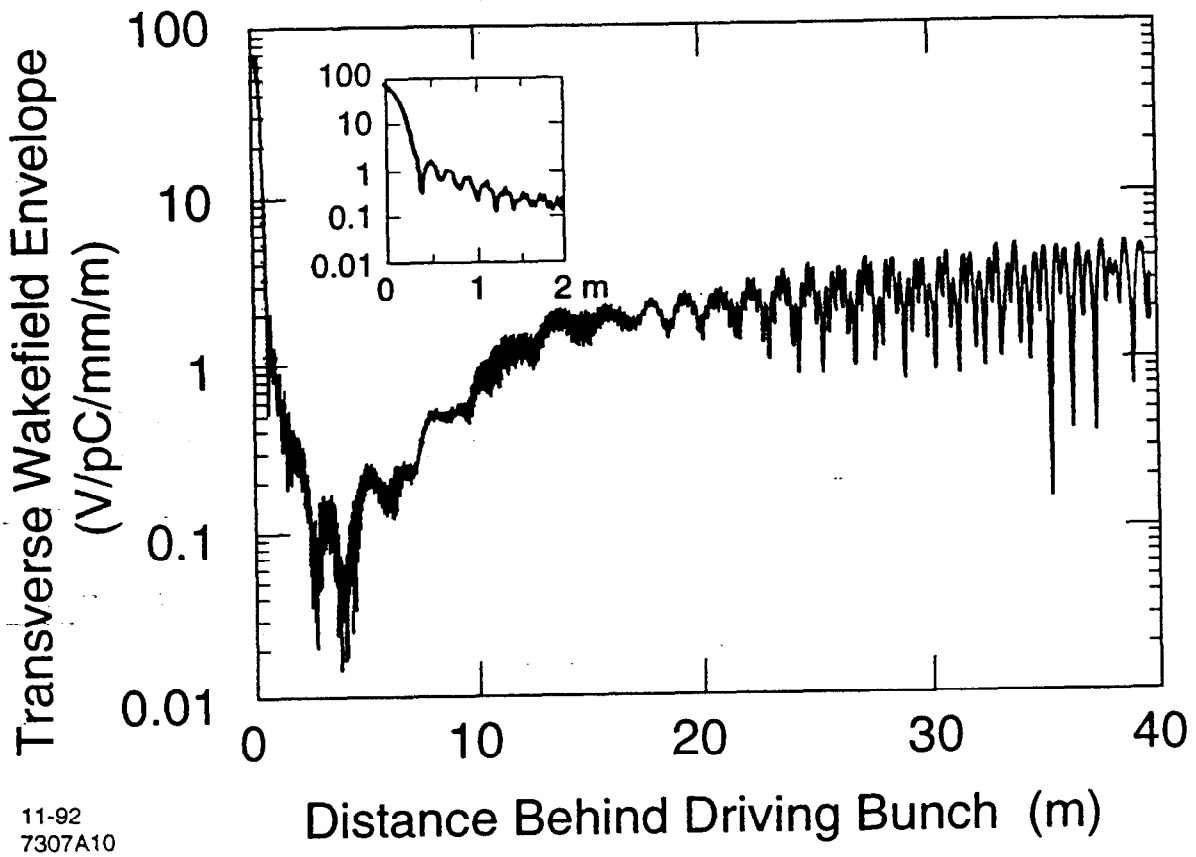

Figure 10. Calculation of the transverse wakefield in an NLCTA accelerator section. (The insert shows the first two meters behind the driving bunch on an expanded distance scale.)

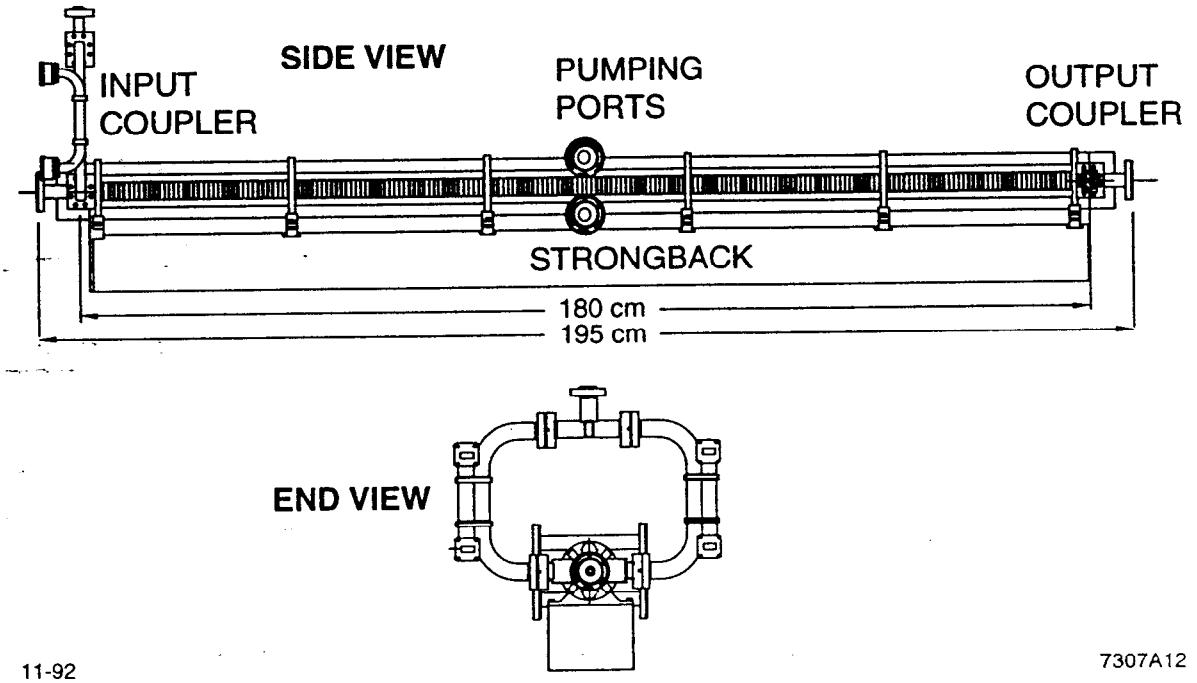

Figure 11. A 1.8-m-long NLCTA accelerator section.

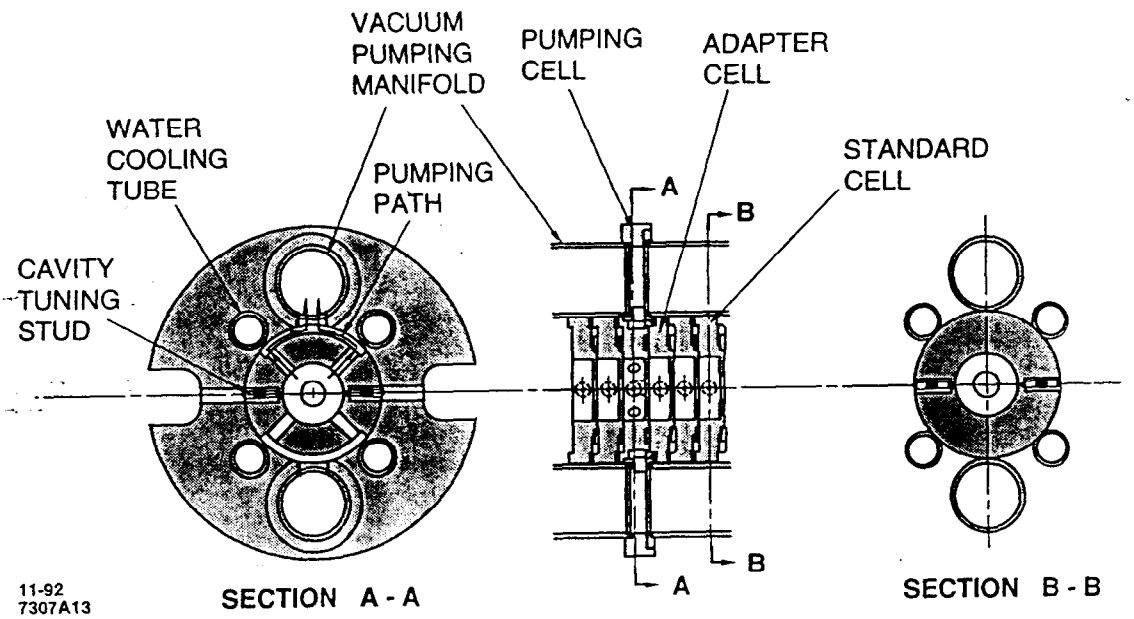

Figure 12. Cells of an NLCTA accelerator section.

in the coupler fields.

Each accelerator section will be mounted on an aluminum strongback. Supports from the strongback to the section will be positioned under the pumping cells, as shown in Figure 11. The support at the input-coupler end will be rigidly attached to the strongback. All other supports will be flexible to allow for longitudinal differential expansion. Each support will permit vertical fine adjustment so that the section can be held straight to within 5 μm.

Field Emission at High Gradients

Theoretical and experimental studies on the behavior of copper accelerator structures under extremely high rf fields have been carried out at SLAC for several years.[18,19] The structures which have been examined recently at X-band are a seven-cell standing-wave (SW) section and a 30-cell traveling-wave (TW) section. Both structures are of the constant-impedance uniform-aperture type with a $\frac{2}{3}\pi$ phase shift per cell at 11.424 GHz. The maximum surface electric field that was reached on the disks exceeded 500 MV/m for the seven-cell SW section. The 30-cell TW section was operated stably at an accelerating gradient of 100 MV/m for an extended period of time. The problems of rf breakdown and "dark current" generated by field emission at high gradient have been studied in considerable detail. The dark current can absorb rf energy, get accelerated, and produce undesirable steering effects, detrimental x-ray radiation, and experimental-physics backgrounds at the final focus. Many experiments have been done to measure the amplitude and spectrum of the dark current and to study phenomena related to rf breakdown such as outgassing, radiation, heating, *etc.* We have concluded that the dark current can be minimized by improving surface finish and cleanliness, and by using gas processing and rf processing.

Figure 13 shows the dark current measured in a Faraday cup as a function of average accelerating field for three stages of rf processing of the 30-cell TW section. The dark current for an accelerating gradient of 50 MV/m was found to be negligible. At 100 MV/m it may be tolerable. We are planning further experimental studies with the full-length NLCTA-prototype sections in the Klystron Test Laboratory and at the NLCTA.

2.6. Transverse Wakefield Effects

We have calculated the multi-bunch beam breakup expected in the NLCTA injector and linac using the methods of Reference 20. The parameters assumed are shown in Table 7. The X-band bunch spacing of the initial NLCTA injector was assumed. Since this spacing is shorter than the decoherence length of the wakefield, the results of the calculation represent a worse case, compared to an NLC-like bunch spacing. The injector will have solenoidal focusing, so the β-function there was assumed to be proportional to the beam energy (E). The β-function in the linac was assumed to be constant at 5 m. A beam loss of 20% was assumed between the injector and the linac.

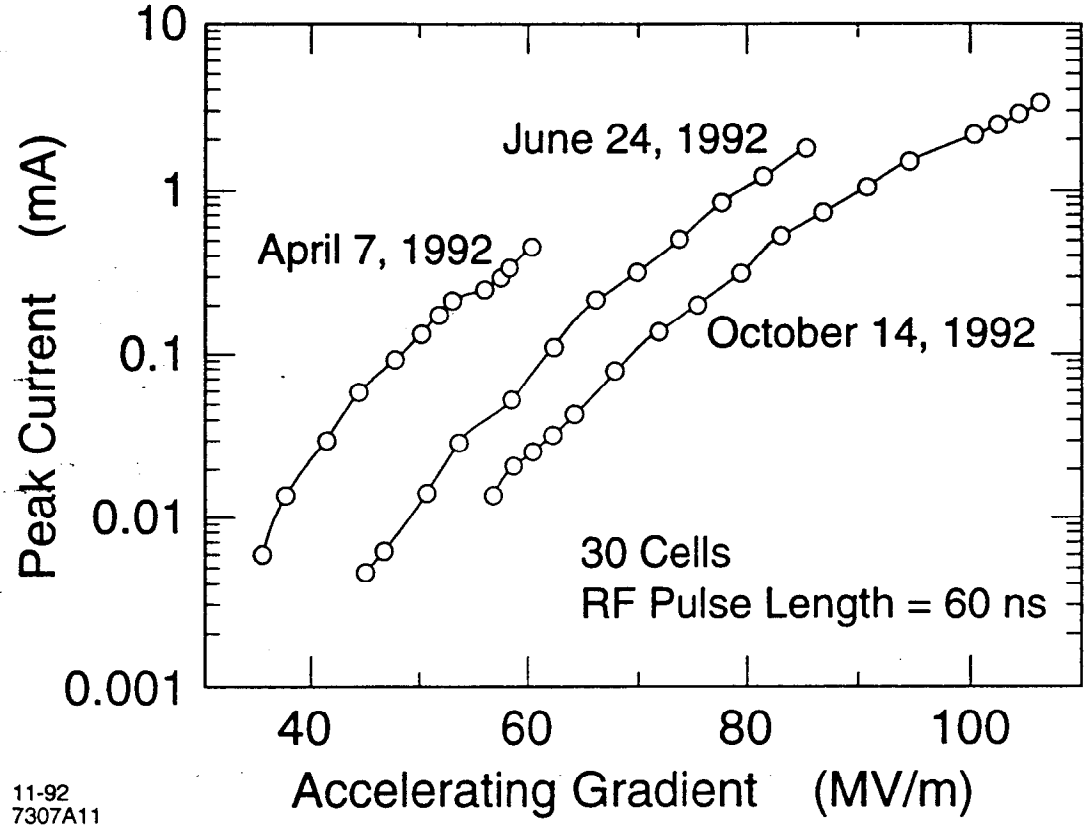

Figure 13. Peak dark current within the pulse measured after three stages of rf processing of the 30-cell traveling-wave section.

In Figure 14(a), we show the factor by which the transverse oscillation amplitude of each bunch has blown up by the end of the injector, assuming that all bunches are injected with the same initial transverse offset, and assuming that the cell-to-cell transverse-mode frequency-detuning distribution of the injector preacceleration section is Gaussian over $\pm 2\sigma$ with $\sigma = 2.5\%$ (as discussed in Section 2.5). The corresponding result if the injector section were not detuned is shown in Figure 14(b). The situation is improved significantly by detuning, as expected. The results of the beam-breakup calculation should be interpreted with some caution because the calculation assumes a fully relativistic beam, which is not the case at the beginning of the injector section, and because the calculation averages the effect of each of the detuned synchronous modes over the whole section, while in reality there are many betatron oscillations within the injector section. We do not expect either of these simplifications to dramatically change the result that the blowup is small in a detuned injector section. However, the actual beam breakup is unlikely to be quite as small as that seen in Figure 14(a).

In Figure 15, we show the factor by which the transverse oscillation amplitude of each bunch has blown up by the end of the detuned linac. Detuning the 1.8-m linac sections is essential for controlling the multi-bunch beam breakup; without detuning, the beam breakup is worse by many orders of magnitude. Since the bunches from the injector are hardly blown up at all (assuming detuning), we have assumed for simplicity that the bunches entering the linac all have the same initial amplitude and phase. In addition to the nominal detuned cell frequency distribution, we have included the effects of random errors in the cell frequencies, with relative errors normally distributed with standard deviation 10^{-4}. The frequency errors have been assumed to be systematic, *i.e.* the same for all the sections, which is the most pessimistic case.

Table 7. Assumptions for the beam-breakup calculation

	Injector	Linac
Initial energy	0.200 MeV	86 MeV
Final energy	86 MeV	500 MeV
Electrons per bunch	5×10^8	4×10^8
β-function	$7 \times 10^{-4}\,\mathrm{m} \times E/(200\,\mathrm{keV})$	5 m
Length	1.8 m	12 m
Bunch spacing	2.624 cm	2.624 cm

Figure 15 shows a very small amplification of an initial transverse beam offset in the NLCTA. This amplification is similar to that obtained in NLC simulations. The

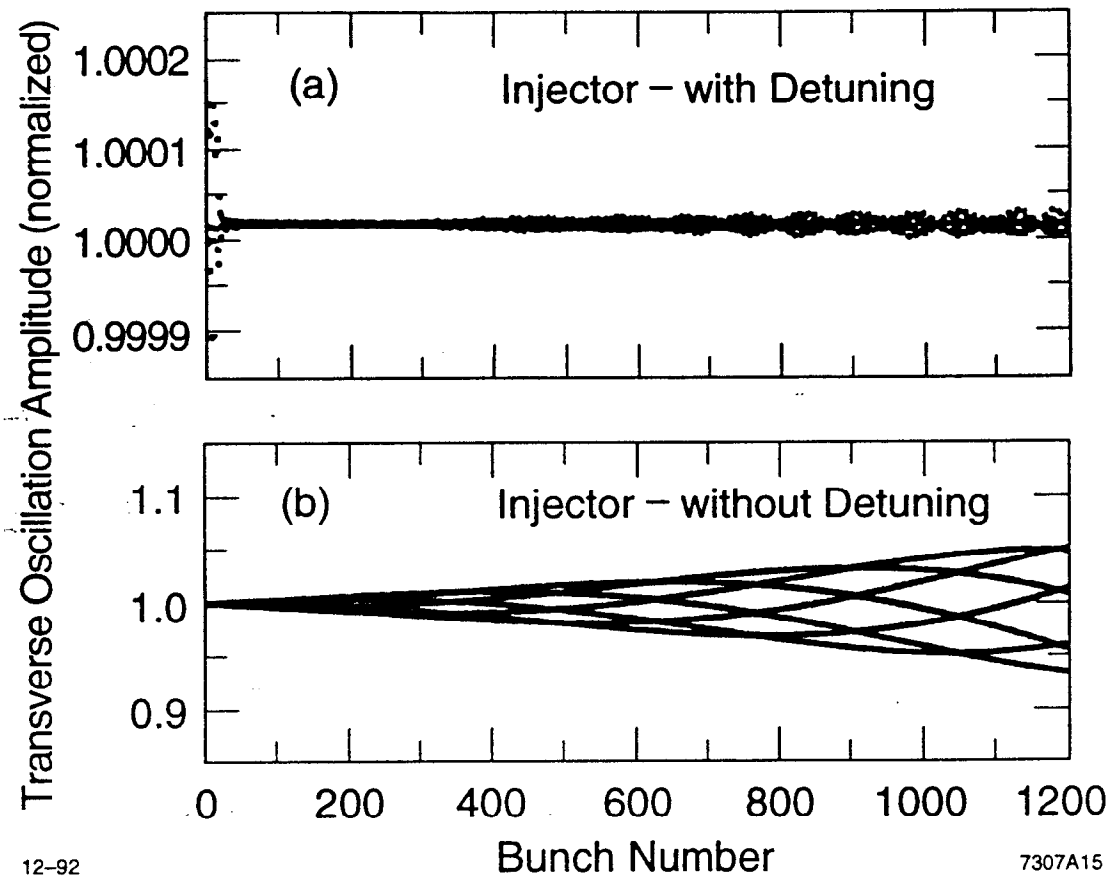

Figure 14. Bunch transverse oscillation amplitudes at end of injector, with and without detuning.

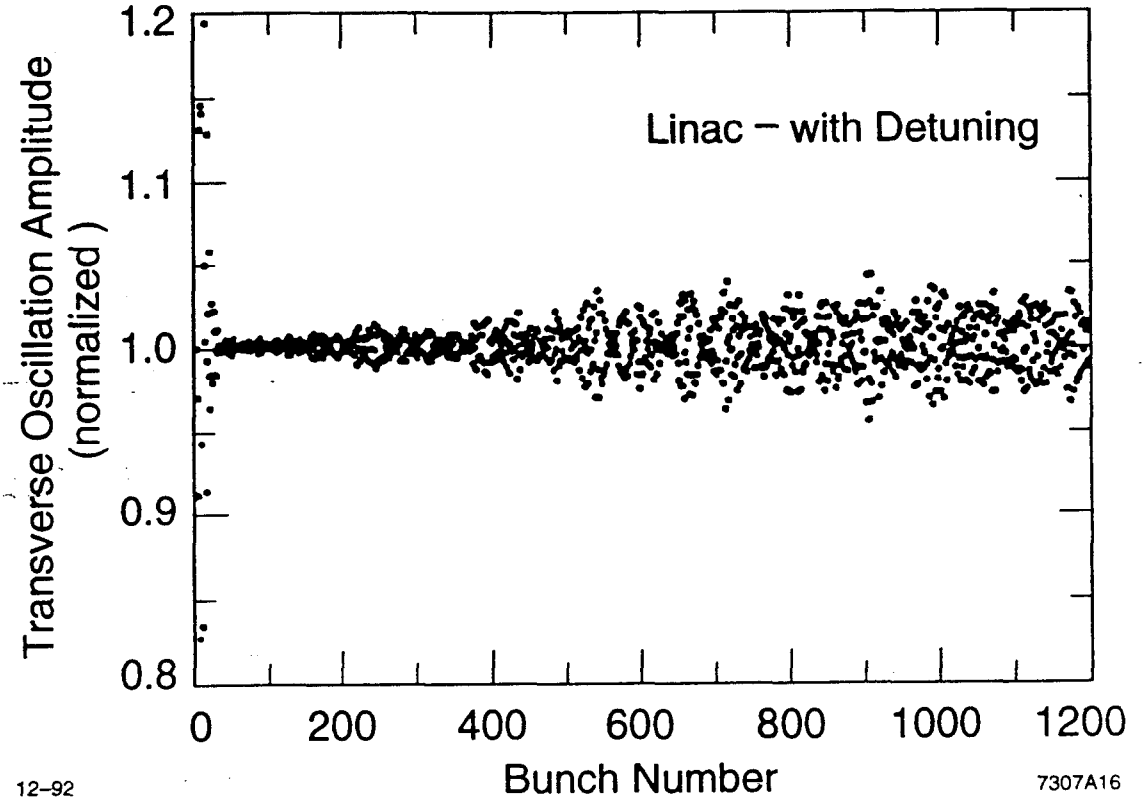

Figure 15. Bunch transverse oscillation amplitudes at end of linac, with detuning.

NLCTA, in spite of its short length, is quite sensitive to transverse wakefields because of its very low beam energy.

2.7. Beam-Loading Compensation

The NLC bunch train is currently expected to be close to one filling time in length, with 0.65×10^{10} electrons per bunch. The relative energy uniformity desired over the bunch train is about 10^{-3}. However, the beam loading, if not compensated, will reach a steady-state value of 25% by the end of the bunch train. The most promising beam-loading energy-compensation strategy for bunch trains of this length is to pre-fill the structure with rf in such a way that the energy gain of each bunch during the transient period approximates the energy gain of each bunch in the steady state. In one implementation of this scheme, the rf pulse is modulated so that the rf electric-field envelope at the input-end of the structure is ramped linearly during one filling time before the bunch train is injected. Since dispersion in the accelerator structure creates large transients on the leading edge of the rf pulse, it is desirable to wait an additional several nanoseconds before injecting the bunch train, to allow the worst of these transients to propagate out of the structure.

A frequency-domain analysis of the above beam-loading compensation scheme is shown in Figure 16, where a 1.8-meter-long accelerating section of the NLCTA is modeled as a constant-gradient structure with filling time of 100 ns, attenuation of 0.517 neper, average elastance* of 900 V/pC/m, and unloaded gradient of 50 MV/m. For the simulation illustrated, a train of bunches, spaced by 1.4 ns (16 rf periods) and containing 0.7×10^{10} electrons per bunch, enters the structure 104 ns after the leading edge of the rf. In Figure 16, the loaded and unloaded energy gain of a test charge is plotted as a function of the time (relative to the leading edge of the rf pulse) the test charge is injected into the structure. The figure shows that the desired compensation to 10^{-3} is achieved in this simulation. Since the detuned structures of the NLCTA are only approximately constant-gradient, it may be desirable or necessary to employ modulation schemes that differ slightly from the linear ramp in rf electric-field envelope to improve the beam-loading energy compensation.

If the bunch train is shorter than about half the filling time, then a "matched filling" technique can be used. In this technique, the bunches are injected before the structure is completely filled, so that the unloaded increase in the accelerating voltage between the arrival times of the bunches approximately cancels the beam loading. One may further improve the compensation by modulating the rf input during the time when the train is passing through the structure, to compensate the small droop in energy that one would otherwise get in the middle of the bunch train.

The initial version of the NLCTA injector will provide a train of bunches with $\frac{1}{16}$ the bunch spacing and $\frac{1}{16}$ the bunch charge of the NLC bunch train. Since the

* Elastance is defined as $\omega R/Q$ per unit length.

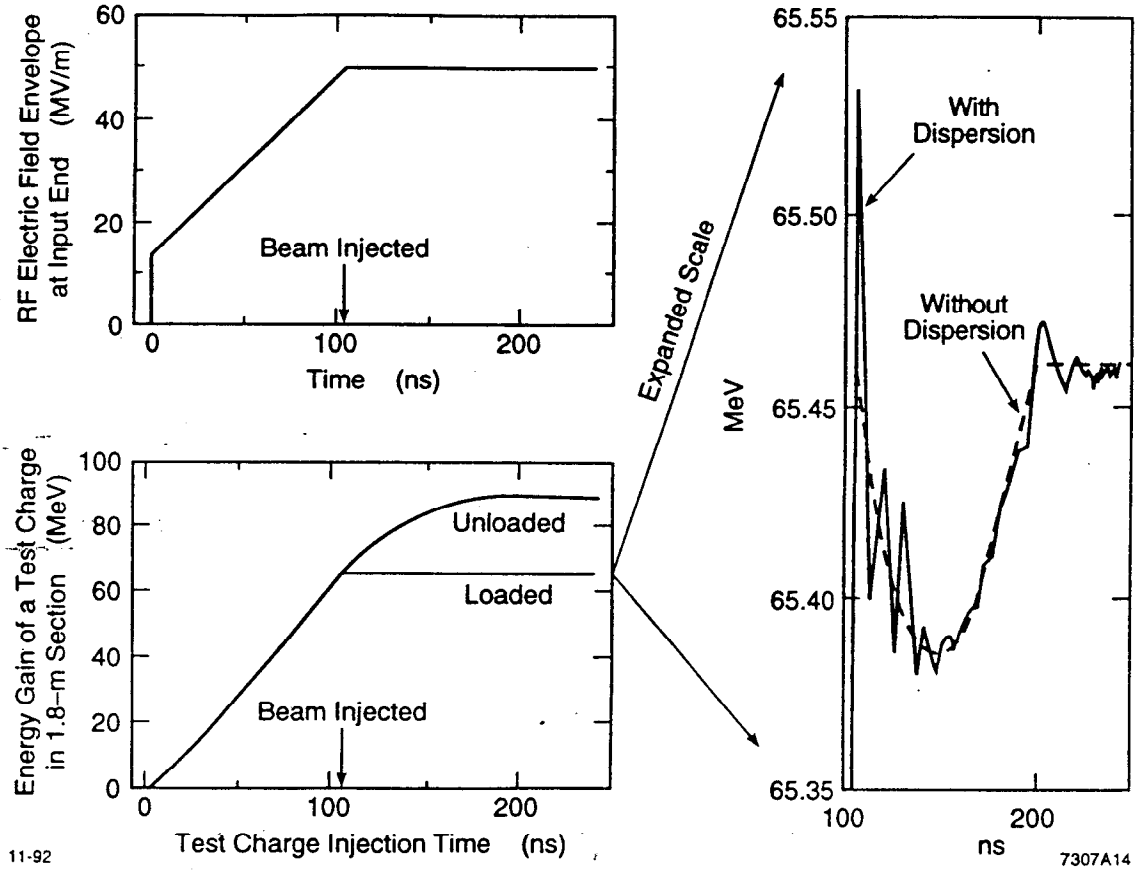

Figure 16. Frequency-domain analysis of a possible beam-loading compensation scheme.

beam-loading depends mainly on the average current, it will be possible to test beam-loading compensation techniques relevant for the NLC with the initial NLCTA bunch train.

2.8. INJECTOR

The design of the NLCTA injector is intended to be the simplest one that will be capable of testing the performance of the NLCTA linac and rf system, particularly with regard to evaluating multi-bunch beam-loading compensation. The design goal was to employ in the injector only very simple, stable, and well-tested technology with outstanding reliability so that the injector would be a well understood tool, rather than a subject of experimentation. Consistent with the goal of simplicity, the bunch spacing will be at the 88-ps period of the accelerating frequency, which is $\frac{1}{16}$ of the NLC design bunch spacing. However, the average current in the NLCTA bunch train will be identical the NLC design so the multi-bunch beam loading in the NLCTA will be nearly identical to the NLC.

The NLCTA injector design comprises the following components:

1. A thermionic-cathode gun with a grid for controlling current and pulse length.
2. An X-band velocity modulation prebuncher followed by a drift in which the bunching occurs.
3. A 0.9-meter-long buncher/capture accelerator section.
4. A second 0.9-meter-long preacceleration section that raises the energy from 45 MeV to 90 MeV.
5. A focusing solenoid which surrounds all the above except the gun.
6. A bucking coil which reduces the magnetic field at the cathode to zero.

The NLCTA injector specifications are listed in Table 8.

The NLCTA injector design incorporates two 0.9-meter-long accelerator sections rather than one of the standard 1.8-meter-long structures for two reasons: (1) The phase of the second section can be adjusted for optimum energy spread within the individual bunches. (2) The beam-loading coefficient is reduced so that the same beam-loading compensation used in the rest of the accelerator is viable for higher currents in the injector. This allows the NLCTA injector to deliver currents that exceed the NLC design specification so that it can deliver the design current after collimation in longitudinal and transverse phase space. (Approximately one-third of injector current is expected to be lost by collimation.)

The injection energy is determined by the requirement of small transverse and longitudinal emittance at the entrance to the linac. Small transverse emittance is required for good beam transport through the small-aperture accelerator sections. Small longitudinal emittance is required in order to meet the bunch-length and energy-spread requirements.

Table 8. NLCTA Injector Parameters

Parameter	NLCTA Design	Injector Upgrade
Gun voltage (kV)	150	
Gun current (A)	2	
Pulse length (ns)	1–140	1–140
Injector unloaded energy gain (MeV)	90	90
Normalized emittance (rad-m)	10^{-4}	$< 10^{-5}$
RMS bunch length (mm)	0.4	0.2
RMS energy spread (%)	0.5	0.2
Bunch frequency (GHz)	11.424	0.714
Bunches per pulse	10–1600	1–100
Electrons per bunch*	0.4×10^9	0.7×10^{10}
Electrons per pulse*	0.7×10^{12}	0.7×10^{12}
Pulse repetition rate (pps)	10	10

*After collimation in the chicane.

In the future, we hope to upgrade the injector to produce a train of bunches similar to that required for the NLC in order to carry out more detailed beam-dynamics studies. Possible specifications for such an upgrade are given in the last column of Table 8. In order to produce the multi-bunch beam, the upgraded injector may use a thermionic-cathode gun with a pulsed grid[21] and subharmonic bunchers. If lower emittance is required, it may be necessary to use a photocathode[22] in an rf gun.[23] The impact of an injector upgrade on the experimental program is discussed in Section 3.7.

2.9. Chicane and Linac Beam Transport

Following the injector will be a pair of "sieve" collimators that will be used to adjust the intensity and maximum transverse size of the bunches. Each of these units will have two insertable slides on which a linear array of different-size collimator patterns are cut. One slide in each pair will contain a set of circular apertures of different radii that will be used to limit the maximum transverse size of the bunches; the other slide in each pair will contain a set of different-size sieve screens that will be used to attenuate the beam intensity without changing the transverse beam size. This attenuation capability will allow the optimization of the beam-loading compensation

in the injector and linac to be decoupled: *i.e.*, once the injector has been set up, the linac intensity then can be adjusted with the sieve, if necessary, to allow for optimum beam-loading compensation without having to re-tune the injector.

To adjust the longitudinal phase space of the bunches, a chicane incorporating four bends will follow the sieve collimators. A collimator with adjustable jaws will be located at a high-dispersion point near the center of the chicane so that the low-energy tail of the bunches can be clipped off. The low-energy tail is due to the combination of the exponentially-shaped longitudinal bunch profile which results from the bunching process, and the subsequent acceleration in the sinusoidal rf field which correlates the longitudinal position and energy of the electrons in the bunches. Hence, cutting off the low-energy tail will shorten the bunch length. To do the collimation, the chicane optics were designed to make the transverse size of the dispersed bunches much larger than that of monochromatic bunches. A horizontal dispersion (η_x) of 35 cm was chosen for the center of the chicane, where β_x and β_y were constrained to be 1 m. At this point, the undispersed rms transverse size of the beam is $\sigma = 0.42$ mm and the transverse size due to dispersion (η times the rms energy spread) is 8.4σ for a 1% rms energy spread.

An adjustable correlation between energy and longitudinal position of the electrons in the bunches will allow a trade-off between energy spread and bunch length. The trade-off involves changing the rf phase in the second 0.9-m-long accelerator section in the injector to achieve the desired energy spread, and then changing the chicane bunch compression (which is represented by the R_{56} element* of the TRANSPORT matrix) to achieve the corresponding minimum bunch length. For such changes we would like the rms energy spread of the bunches to be less than 1% so that the emittance blowup in the chicane due to chromaticity and second-order dispersion is not too large (less than 15%). We would like the intra-bunch energy spread in the spectrometer at the end of the linac to be less than 1% to make it easier to discern bunch-to-bunch energy differences down to the 0.1% level for the multi-bunch beam-loading compensation studies. Achieving this energy spread in the spectrometer will require that the bunch length in the linac is less than 0.5 mm.

However, the price for bunch compression is greater than just increased intra-bunch energy spread in the chicane. The chicane, when set for bunch compression ($R_{56} \neq 0$), will convert bunch-to-bunch energy differences from the injector into bunch-phase differences with respect to the accelerating wave, which will then be converted into energy differences in the linac. These energy differences will make it harder for us to study beam-loading compensation. Fortunately, we can make the chicane isochronous ($R_{56} = 0$) to avoid this problem, and we can still meet the longitudinal phase-space requirements. One way to do this is to set the chicane collimator to limit the full bunch length to 1.5 mm, which will transmit about 70% of the electrons, and will result in an rms bunch length of 0.4 mm and a minimum rms energy spread of about

* The path-length difference for two relativistic particles is R_{56} times their relative energy difference.

0.5%. The plan is to operate with these parameters although we have allowed enough flexibility in the design of the chicane so that, if the bunch-to-bunch energy differences can be tolerated, the quadrupole settings in the chicane can be adjusted to give the desired bunch compression. For example, the bunch length can be halved to 0.2 mm with $R_{56} = -10\,\mathrm{mm}$; however, in this case the energy spread in the chicane would double to 1%.

To achieve isochronicity ($R_{56} = 0$), the nominal chicane lattice was designed[24] so that the phase advance between adjacent bends is 180°, and hence the dispersion goes though zero at each of the bends. This requires a rather large total phase advance, and therefore a large number of quads. In addition, the spacing between quads must be fairly large to prevent rapid changes in the β-function, and to accommodate beam-diagnostic instrumentation. The resulting design has a total of 12 quads, each 15 cm long, spaced over a distance of 5.4 m between the first and last bend. Also, four quads are used upstream of the chicane to match from the optics of the injector, where it is assumed that $\beta_x = \beta_y = 0.35$ cm and $\alpha_x = \alpha_y = 0$ at the exit of the injector solenoids. Likewise, four quads are used to match to the linac optics. Specific sets of quad settings have been computed which achieve values of R_{56} in the range from -7.5 cm to $+2.5$ cm, including the isochronous case where $R_{56} = 0$.

A study of the sensitivity of the R_{56} matrix element of the chicane to errors in the magnetic field strengths was done using the program DIMAD. Errors were introduced by changing the strength of individual quads and bends by 1% in the DIMAD input describing the chicane. The isochronicity is rather well preserved; the R_{56} variation resulting from each error that was introduced is less than 1.5 mm, which is small compared to the 10-mm tolerance on R_{56}.

The linac optics were designed[24,25] to keep the transverse beam size small compared to the apertures of the accelerator structures, which vary from 5.7 mm to 3.9 mm in radius. A constraint in reducing the β-function for this purpose is the 1.8-m length of the accelerator structures since the quads will only be placed between the structures. A FODO lattice with about 100° of phase advance per cell was chosen which yields a maximum β of approximately 8 m and a worst-case beam stay-clear of 5σ. This lattice design also takes into account the rapid beam-energy gain along the linac, which is expected to be 50 MeV/m (unloaded) for the initial running.

The lattice functions and the rms beam size for the isochronous chicane and linac are shown in Figure 17.

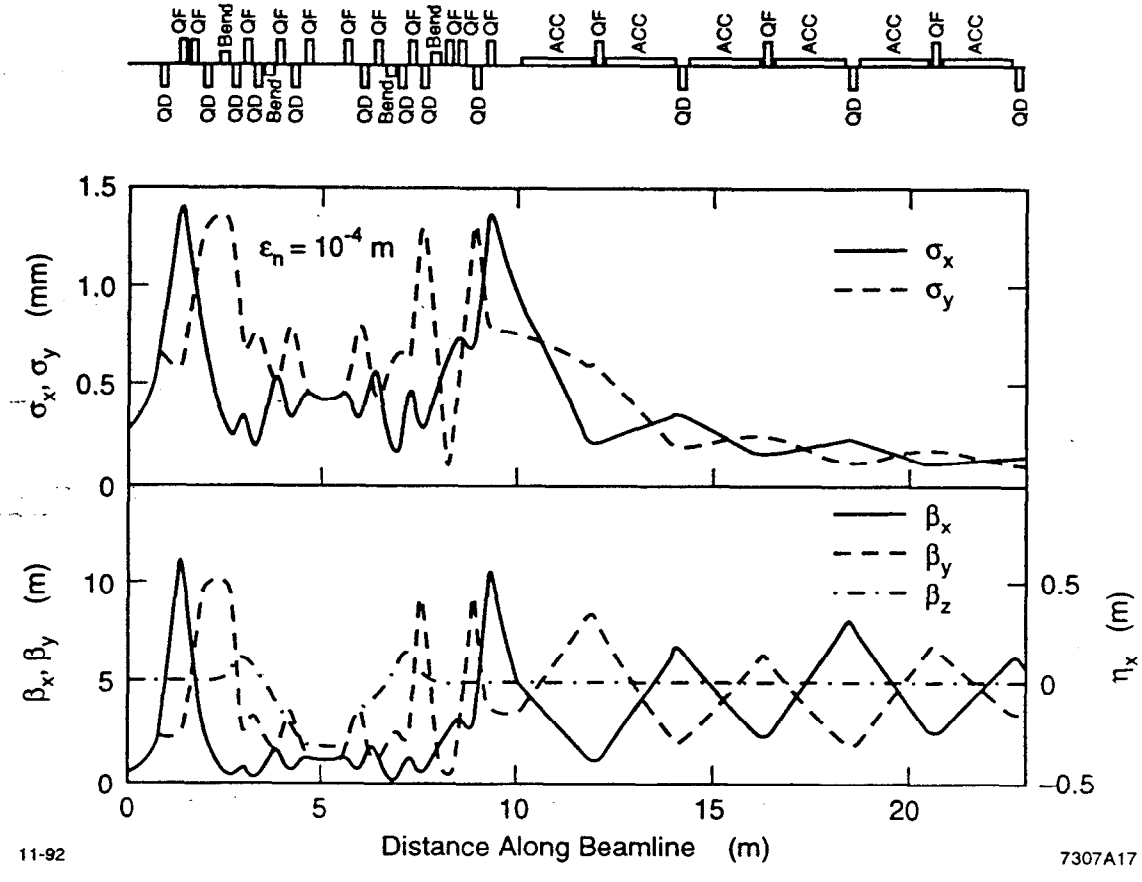

Figure 17. Beam size and lattice functions along the isochronous chicane and linac.

2.10. SPECTROMETER

A matching section and spectrometer downstream of the last linac section will allow measurements of the energy and phase-space density of the bunch train with time-resolution of approximately 1 ns, corresponding to sets of 11 bunches in the design injector's 11.424-GHz bunch train, or to individual bunches in an upgraded injector's 0.714-GHz bunch train.

The spectrometer utilizes a dipole "C"-magnet which will steer the beam by 12° into a high-dispersion line, or permit the use of a straight-ahead line. Figure 18 shows the lattice of the spectrometer that will follow directly after the last linac section, continuing from the 23-meter point of Figure 17. (The figure shows the high-horizontal-dispersion line.) There are two FODO cells to measure and match the incoming beam down to asymmetric double concave waists with $\beta_x = 0.04\,\mathrm{m}$ and $\beta_y = 0.50\,\mathrm{m}$ at the point 4.6 m downstream from the linac. The pole shapes of the bend magnet and the two additional quadrupoles of the spectrometer focus the beam at PM2 ($\beta_x = 0.24\,\mathrm{m}$ and $\beta_y = 0.50\,\mathrm{m}$), located 5 m downstream from the bend.

At the focal point, the horizontal dispersion ($\eta_x = 1.1\,\mathrm{m}$) and the β-function ($\beta_x = 0.24\,\mathrm{m}$) yield a first-order resolving power,

$$RP_1 = \frac{\eta_x}{\sqrt{\beta_x \epsilon_x}} = 8 \times 10^3 \left(\frac{626\,\mathrm{MeV}}{E}\right)^{1/2} \left(\frac{10^{-4}\,\mathrm{m\text{-}rad}}{\epsilon_n}\right)^{1/2}.$$

This value is only slightly worse when computed using third-order TURTLE with full Gaussian distributions. For an energy spread of $\pm 0.4\%$ in a bunch, there is an increase of less than 10% in the rms transverse beam sizes when we kick the nominal bunch vertically by $\pm 6.6\,\mathrm{mrad}$ using the kicker described below.

A pulsed dipole kicker magnet (VKICK in Figure 18) will separate the bunches vertically for momentum analysis. We plan to use an existing SLC damping ring kicker whose phase, strength, and rise-time can be varied. A dipole steering magnet (YCOR in Figure 18) will allow the distribution of kicked bunches to be centered about the central design orbit. Beam profile monitors (PM1 and PM2 in Figure 18) and wire scanners (not shown) will be used to measure bunch size. A strip-line beam-position monitor (BPM) will be associated with each quadrupole magnet.

The straight-ahead line will be used to measure the undispersed bunch size and position. Its aperture will be made large enough to allow coarse energy measurements with the spectrometer magnet partially powered. Both the straight-ahead line and the high-dispersion line terminate in heavily-shielded beam dumps.

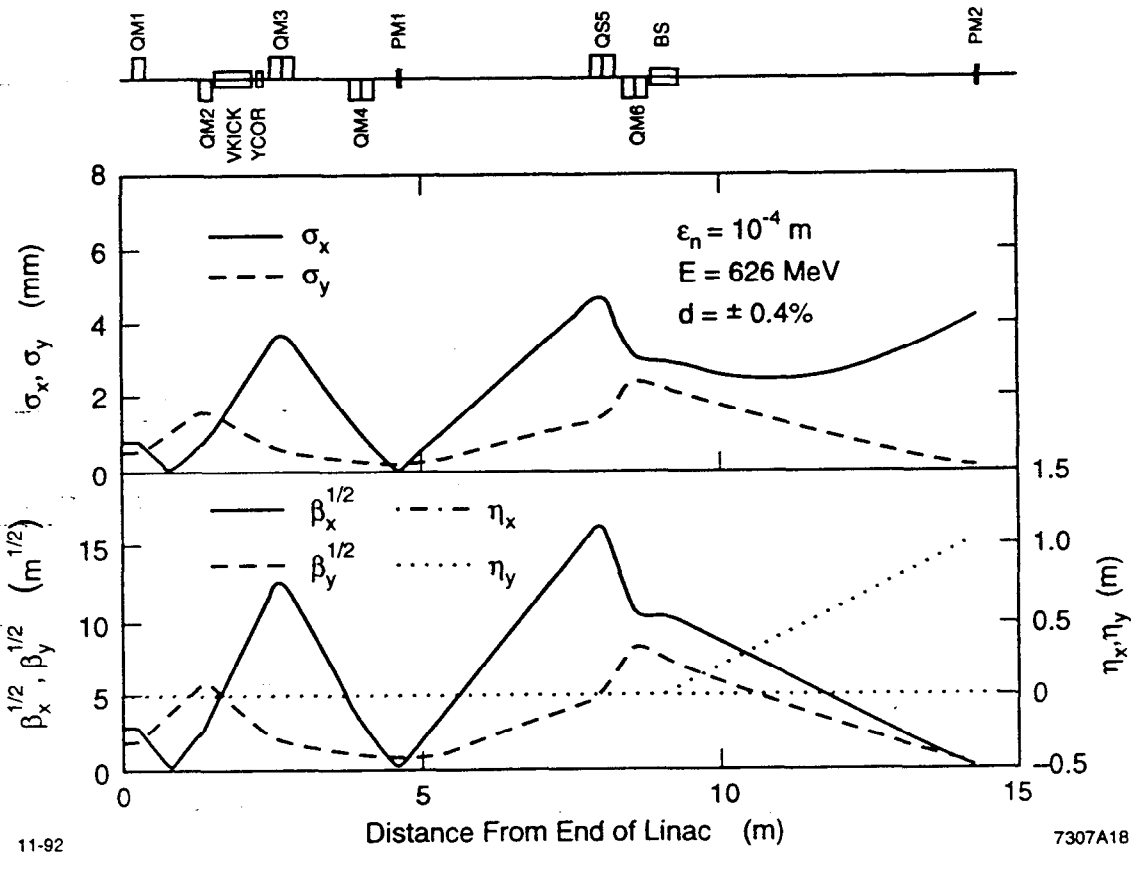

Figure 18. Beta-functions and rms beam size in the matching section and spectrometer.

3. Experiments

The goal of the NLCTA experimental program is to measure the performance characteristics of the multi-section X-band linac and high-power rf systems. The experiments will go beyond the work with single power sources and structures in the Klystron Test Laboratory; the NLCTA beam will be much better defined and much more precisely analyzed, both before and after acceleration. In addition to system operations tests, beam-dynamics studies will be done using three types of bunch trains: a short bunch train of a few nanoseconds will be used to measure the unloaded energy-gain characteristics of the linac, a variable-length bunch train will be used to measure field-emission currents in the linac with and without injected beam, and the nominal 150-ns-long bunch train will be used to test multi-bunch beam-loading compensation. The specifics of these experiments are discussed in the following sections, concluded by a discussion of other types of wakefield studies that will be made possible by upgrading the NLCTA injector. Although we will not elaborate on it further, an important part of the experimental program, of great relevance for future linear colliders, is the commissioning of the multi-bunch beam instrumentation.

3.1. System Studies

The NLCTA rf system was designed to be large enough in scale, with four klystrons powering eight structures through four SLED-II rf pulse compressors, that it will serve to test system control and monitoring methods applicable to NLC-scale linacs. A key component of the monitoring system will be instrumentation that can detect and digitize the phase and amplitude envelopes of the 250-ns-long rf pulses. This waveform sampling system, which will be based on commercially available high-speed waveform digitizers, is intended to resolve 0.1% amplitude and 0.1° phase variations on time-scales greater than about 5 ns. The data acquisition will be controlled by local microprocessors, one of which will be assigned to each rf station,* in order to permit parallel, high-level processing of the data.

We plan to monitor the transmitted and reflected rf pulses at many points along the route between each klystron and its associated accelerator structures. There will be two waveform digitizers per rf station, into which the rf phase and amplitude signals from the monitor points can be multiplexed. In this way, correlations between any two signals can be examined. An important function of the monitoring system will be to characterize the stability of the rf pulses. For this purpose, the signals will be processed in three basic ways. To characterize the short-term stability of some aspect of the waveform, a few hundred consecutive pulses will be sampled and analyzed. To monitor long-term stability, a sample will be taken every few minutes and stored in

* An rf station is defined as one klystron, its SLED-II pulse compressor, and its pair of accelerator structures.

history buffers. Finally, to monitor rare occurrences, the system will be set up to continuously sample every pulse, but will save only a portion of the data associated with distinguishable events.

3.2. Unloaded Energy Gain

To measure the unloaded energy gain characteristics of the linac, only one klystron will be run at a time. A short bunch train, which makes the beam loading negligible, will be used to simplify the measurement. The energy gain of the bunch train depends on the rf waveform entering the two energized structures, on the rf transmission properties of the structures, and on any field emission (or breakdown) that occurs in the structures. The rf transmission properties of the structures have been computed[26] so that, from a measurement of the input rf waveform, one can predict how the ideal energy gain should vary as a function of the transit time of the bunch train relative to the rf pulse. By comparing this calculation to measurements done at low rf-power levels, we will test our theoretical understanding of the rf transmission properties of the accelerator sections. By comparing low- and high-power measurements, we will look for effects from field emission within the structures. Checks for field emission will also be made by observing the energy-gain stability at a fixed transit time for different rf power levels.

3.3. Linac Field-Emission Current

In addition to over-loading individual structures, there is a concern that field emission currents will be accelerated sufficiently to be captured by the accelerating wave and transported in an NLC-like linac. To investigate this possibility, and to provide more data on field-emission activity in the structures, the NLCTA linac will be instrumented with two types of detectors. An extended scintillation counter will be placed alongside each of the structures to provide a measure of the expelled (uncaptured) field-emission current, and a resistive wall monitor will be installed in the beam line at the beginning, middle and end of the linac. The time-resolution of the scintillation counters will be approximately 20 ns. The time-resolution of the resistive wall monitor will be approximately 1 ns.

With the beam off, we will measure the expelled and transported current signals as functions of the rf power and of the strengths of the intervening quadrupole and dipole magnetic fields. With a strong dipole field, any wall monitor currents should be due only to field emission in the structures immediately upstream. By observing the change in the currents with no dipole field, but with different-strength quadrupole configurations, we will characterize the transport of field-emission current in the linac. Although the quadrupole field strengths available in the NLCTA will not be as great as the strengths that will be used in an NLC main linac, we believe that they will be sufficient to fully suppress the transport of the field-emission current. Studies will also be done to measure how much of the field-emission activity is associated with

the presence of the beam by varying the length of the bunch train and observing the change in the time-structure of the monitor signals.

3.4. Multi-Bunch Beam-Loading Compensation

One of the goals of the NLCTA is to demonstrate that multi-bunch beam-loading compensation can be readily maintained at the 0.1% level for a beam current yielding a steady-state loading of 25%. To achieve the compensation, the shape and/or timing of the rf pulses will be adjusted so that the resulting change in unloaded energy gain along the bunch train offsets the energy loss from the loading. Demonstrating compensation at the 0.1% level will require careful preparation of the bunch train so as not to generate other sources of bunch-to-bunch energy differences. The bunch train injected into the linac will be checked for tolerances on the uniformity of bunch energy, intensity, and spacing. To measure the degree of compensation, the bunch train will be analyzed in the spectrometer using a vertical kicker magnet, as described in Section 2.10. From the measurements of the rf waveform entering the structures, and from our theoretical understanding of the rf transmission through the structures,[26] we should be able to predict the gross features of the bunch-to-bunch energy differences that are observed.

The specific method for shaping the rf waveforms has not yet been selected. Although we will probably modulate the amplitude of the rf drive to the klystrons, various types of rf phase modulation prior to SLED-II pulse compression are also options to be tried. The rf must be stable in time, whichever method we choose. Maintaining the stability of the rf pulses may require feeback which should be relatively straightforward to implement in the rf control system that is envisioned for the NLCTA.

3.5. Transverse Components of the Accelerating Field

The tolerances on the allowable transverse components of the accelerating field in the structures of an NLC linac are fairly tight compared to SLC standards. These tolerances differ depending on whether the transverse electric field is in-phase or 90° out-of-phase with the bunches, and on whether the field jitters from pulse to pulse or is static. In the NLCTA, we will be able to measure transverse electric-field components with resolution on the order of, or smaller, than the NLC tolerances.

The basic approach in these measurements is to vary the phase of one klystron at a time and to record the change in the bunch trajectories using the BPMs downstream from the associated pair of structures. Fitting the amplitudes of the observed betatron oscillations to a sinusoidal function of the klystron phase will yield the in-phase and out-of-phase static components of the accelerating field. To measure the jitter in these components, the pulse-to-pulse rms variation of the induced betatron motion will be computed with the klystron on and off, and at the in-phase and out-of-phase settings.

To obtain accurate results will require special attention to how the data are taken. A short bunch train will be used, only one linac klystron will be powered at a time, and the quadrupoles will be turned off downstream of the associated structures so that bunch energy changes do not produce trajectory changes. The measured outgoing trajectory will be corrected pulse-to-pulse to account for any changes in the incoming trajectory. This correction will be based on the trajectory fit to the BPM data in the region between the center of the chicane and the structures being powered. With this procedure, a resolution of about 0.2 keV in the transverse accelerating field should be achieved.

The out-of-phase component of the transverse field, which will degrade the bunch emittance in the NLC due to the differential kick it produces along the length of the bunch, should be less than 1 keV to keep the emittance growth below 10%. Therefore both static and jitter components of this magnitude should be discernable in the NLCTA. Jitter in the in-phase component of the transverse field will also lead to emittance growth in the NLC, as a result of the dispersion it generates. The tolerance for a 10% growth is much smaller, about 0.2 keV, so we will not be able to put tight limits on the NLC emittance growth from this mechanism if indeed no jitter is observed.

A static in-phase component of the transverse field is fairly benign since its effect can be offset with a dipole magnet. Coupled with jitter in the energy gain, however, it also contributes to the emittance growth in the same manner as in-phase jitter. A 1% jitter in energy gain, which is reasonable for the klystrons being developed, yields a tolerance 100 times larger, or 20 keV, on the static in-phase component. Our resolution for measuring this component is also much larger since an absolute measure of the bunch angular trajectories relative to the structure axes are needed to correct the measurement for the transverse field component due to off-angle trajectories. For this correction, we will rely on the absolute BPM calibration and on the BPM alignment to the structure axes, each of which will be known to about 100 μm. These errors translate into a 10-keV uncertainty in the static field strength so, again, the measurement resolution is near the tolerance.

3.6. Transverse Multi-Bunch Beam Breakup

The NLCTA (like the NLC) would not operate stably if conventional constant impedance accelerator structures were used. In both cases the offset of the bunches would be amplified by many orders of magnitude by the end of the linac. The detuned structures for the NLCTA will eliminate this blowup. This will be tested experimentally using the straight-ahead line of the spectrometer and the vertical kicker magnet.

Using corrector magnets in the chicane, the bunch train will be launched into the linac with a horizontal position or angle offset. The resulting positions of the bunches exiting the linac will be measured using a profile monitor in the straight-ahead line of the spectrometer in conjunction with the vertical kicker. This will allow us to

distinguish the bunches along the train by their vertical offset while observing the amplification of the initial horizontal betatron amplitude.

3.7. Studies with an Upgraded Injector

There are a number of NLC linac beam-dynamics issues which cannot be readily addressed with the initial NLCTA injector. The small bunch intensity produced by the X-band injector makes single-bunch longitudinal- and transverse-wakefield effects too small to be measured easily. Also, the small bunch spacing makes it difficult to accurately measure the strength of the long-range transverse wakefield from its effect on betatron motion. As discussed in Sections 2.1 and 2.8, we hope to upgrade the injector in the future to produce NLC-like bunch trains with 0.65×10^{10} electrons per bunch and 1.4-ns bunch spacing. If a photocathode rf gun is used, we may be able to produce an adjustable-length bunch train (from 1 to 100 bunches) with a fairly small normalized (invariant) emittance ($\epsilon_n < 10^{-5}$ m-rad) and NLC-like bunch lengths (100 μm after compression).

With such an injector operating in a single-bunch mode, the mean energy of the bunch in the spectrometer would be measured as a function of bunch intensity to infer the short-range longitudinal wakefield strength. The size of this quantity is of particular interest since it has some theoretical uncertainty for such short bunches. Similarly, the strength of the short-range transverse wakefield would be inferred by measuring the change in the transverse bunch profile, using the wire scanner before the spectrometer bend, as a function of bunch intensity and betatron amplitude in the linac. To study the long-range transverse wakefields, a long bunch train would be used and the effects of the wakefields on the betatron motion of the bunches in the linac would be measured.

Until a new injector is built, some of these issues will be addressed with the Accelerator Structure SET-up (ASSET) facility at the SLC. ASSET will be built into the SLC to allow measurements of the wakefield characteristics of a single un-energized accelerator structure. In particular, ASSET is optimized to measure the long-range transverse wakefield to verify the suppression expected from the detuning of the X-band accelerator structures, as shown in Figure 10.

References

1. Burton Richter, "From the SLAC Linear Collider to the Next Linear Collider: A Status Report and Road Map" (SLAC-PUB-5736, February 1992); Ronald D. Ruth, "The Development of the Next Linear Collider at SLAC" (SLAC-PUB-5729, February 1992); both papers to be published in *Proceedings of the Workshop on Physics and Experiments with Linear Colliders*, Saariselka, Finland, September 9–14, 1991.

2. Ronald D. Ruth, "The Next Linear Collider" (SLAC-PUB-5406, February 1991), published in *Proceedings of the 18th Annual SLAC Summer Institute on Particle Physics: Gauge Bosons and Heavy Quarks*, Stanford, California, 1990, edited by Jane F. Hawthorne (SLAC Report No. 378, Stanford, 1991), pp. 143–164; also published in *Proceedings of the Joint US-CERN Particle Accelerator School on the Frontiers of Particle Beams: Intensity Limitations*, Hilton Head, South Carolina, November 7–14, 1990, edited by M. Dienes, M. Month, and S. Turner (Springer-Verlag, New York, 1992).

3. *Proceedings of the Third International Workshop on Linear Colliders*, BINP, Protvino, USSR, September 17–27, 1991, edited by V. Balakin, S. Lepshokov, and N. Solyak (BINP, Protvino, 1990).

4. *Proceedings of the 2nd International Workshop on Next-Generation Linear Collider*, KEK, Tsukuba, Japan, March 28–April 5, 1990, edited by S. Kurokawa, H. Nakayama, and M. Yoshioka (KEK Internal Report 90-22, 1990).

5. *Proceedings of the International Workshop on Next-Generation Linear Colliders*, SLAC, Stanford, California, November 28–December 9, 1988 (SLAC Report No. 335, 1988).

6. J. M. Paterson, R. D. Ruth, C. Adolphsen, K. L. Bane, D. L. Burke, R. S. Callin, G. Caryotakis, R. L. Cassel, S. L. Clark, H. Deruyter, K. Fant, R. W. Fuller, S. A. Heifets, H. A. Hoag, R. Humphrey, A. J. Keicher, S. Kheifets, R. F. Koontz, N. M. Kroll, T. L. Lavine, G. A. Loew, A. Menegat, R. H. Miller, C. Nantista, M. E. Nordby, C. Pearson, J. Rifkin, J. Spencer, S. G. Tantawi, K. A. Thompson, A. E. Vlieks, V. Vylet, J. W. Wang, P. B. Wilson, A. D. Yeremian, and B. Youngman, "The Next Linear Collider Test Accelerator" (SLAC-PUB-5928), to be published in *Proceedings of the 15th International Conference on High-Energy Accelerators*, Hamburg, Germany, July 20–24, 1992.

7. P. B. Wilson, Z. D. Farkas, N. M. Kroll, T. L. Lavine, A. Menegat, C. Nantista, and R. D. Ruth, "Progress at SLAC on High-Power RF Pulse Compression" (SLAC-PUB-5866), to be published in *Proceedings of the 15th International Conference on High Energy Particle Accelerators*, Hamburg, Germany, July 20–24, 1992.

8. N. M. Kroll, Z. D. Farkas, T. L. Lavine, A. Menegat, C. Nantista, R. D. Ruth, and P. B. Wilson, "A High Power SLED-II Pulse Compression System"

(SLAC-PUB-5782), published in *Proceedings of the Third European Particle Accelerator Conference*, Berlin, Germany, March 24–28, 1992, edited by H. Henke, H. Homeyer, and Ch. Petit-Jean-Genaz (Editions Frontières, Gif-sur-Yvette, France, 1992), pp. 327–329.

9. P. B. Wilson, Z. D. Farkas, and R. D. Ruth, "SLED II: A New Method of RF Pulse Compression" (SLAC-PUB-5782), published in *Proceedings of the 1990 Linear Accelerator Conference*, Albuquerque, New Mexico, September 10–14, 1990 (Los Alamos National Laboratory Report LA-12004-C, 1991), pp. 204–206.

10. T. L. Lavine, Z. D. Farkas, A. Menegat, R. H. Miller, C. Nantista, G. Spalek, and P. B. Wilson, "High-Power Radio-Frequency Binary Pulse-Compression Experiment at SLAC" (SLAC-PUB-5451), published in *Proceedings of the 1991 IEEE Particle Accelerator Conference*, San Francisco, California, May 6–9, 1991 (IEEE Catalog No. 91CH3038-7), pp. 652–654.

11. A. E. Vlieks, R. S. Callin, G. Caryotakis, K. S. Fant, W. R. Fowkes, T. G. Lee, and E. L. Wright, "100-MW Klystron Development at SLAC" (SLAC-PUB-5480), published in *Proceedings of the 1991 IEEE Particle Accelerator Conference*, San Francisco, California, May 6–9, 1991 (IEEE Catalog No. 91CH3038-7), pp. 798–800.

12. G. Caryotakis, "Multimegawatt RF Power Sources for Linear Colliders" (SLAC-PUB-5508), published in *Proceedings of the 1991 IEEE Particle Accelerator. Conference*, *op. cit.*, pp. 2928–2932.

13. K. Harris, J. de Lamare, V. Nesterov, and R. Cassel, "600-kV Modulator Design for the SLAC Next Linear Collider Test Accelerator" (SLAC-PUB-5851), to be published in *Proceedings of the 20th International Power Modulator Symposium*, Myrtle Beach, South Carolina, June 23–25, 1992.

14. H. Deruyter, Z. D. Farkas, H. Hoag, K. Ko, N. M. Kroll, G. A. Loew, R. H. Miller, R. B. Palmer, J. M. Paterson, K. Thompson, J. W. Wang, and P. B. Wilson, "Damped and Detuned Accelerator Structures" (SLAC-PUB-5322), published in *Proceedings of the 1990 Linear Accelerator Conference*, Albuquerque, New Mexico, September 10–14, 1990 (Los Alamos National Laboratory Report LA-12004-C, 1991), pp. 132–134.

15. J. W. Wang, G. A. Loew, J. W. Simpson, E. Chojnacki, W. Gai, R. Konecny, and P. Schoessow, "Wakefield Measurements of SLAC Linac Structures at the Argonne AATF" (SLAC-PUB-5498), published in *Proceedings of the 1991 IEEE Particle Accelerator Conference*, San Francisco, California, May 6–9, 1991 (IEEE Catalog No. 91CH3038-7), pp. 3219–3221.

16. R. H. Miller, C. Adolphsen, K. L. Bane, H. Deruyter, Z. D. Farkas, R. L. Gluckstern, H. Hoag, N. Holtkamp, K. Ko, N. M. Kroll, T. L. Lavine, G. A. Loew, E. M. Nelson, R. B. Palmer, J. M. Paterson, R. D. Ruth, K. Thompson, A. E. Vlieks, J. W. Wang, and P. B. Wilson, "Accelerator Structure Work

for NLC" (SLAC-PUB-5865), to be published in *Proceedings of the 15th International Conference on High Energy Accelerators*, Hamburg, Germany, July 20–24, 1992.

17. K. L. F. Bane and R. L. Gluckstern, "The Transverse Wakefield of a Detuned X-Band Accelerator Structure" (SLAC-PUB-5783), submitted to *Particle Accelerators.*

18. G. A. Loew and J. W. Wang, "RF Breakdown Studies in Room Temperature Electron Linac Structures" (SLAC-PUB-4647, May 1988), published in *Proceedings of the 13th International Symposium on Discharges and Electrical Insulation in Vacuum*, Paris, France, June 27–30, 1988, edited by J. M. Buzzi and A. Septier (Editions de Physique, Les Ulis, France, 1988).

19. J. W. Wang, R. A. Curry, H. Deruyter, H. A. Hoag, R. F. Koontz, G. A. Loew, A. Menegat, R. H. Miller, R. D. Ruth, A. E. Vlieks, C. Yoneda "High Gradient Studies on 11.4-GHz Copper Accelerator Structures" (SLAC-PUB-5900, August 1992), to be published in *Proceedings of the 1992 Linear Accelerator Conference*, Ottawa, Ontario, Canada, August 23–28, 1992.

20. K. Thompson and R. D. Ruth, "Controlling Transverse Multi-bunch Instabilities in Linacs of High Energy Linear Colliders," *Physical Review D41*, 964 (1990).

21. T. Naito, M. Akemoto, H. Akiyama, H. Hayano, H. Matsumoto, J. Urakawa, and M. Yoshioka, "Generation of Multi-Bunch Beam with Thermionic Gun for the Japan Linear Collider" (KEK preprint 92-97), to be published in *Proceedings of the 1992 Linear Accelerator Conference*, Ottawa, Ontario, Canada, August 23–28, 1992.

22. P. G. O'Shea, S. C. Bender, B. E. Carlsten, J. W. Early, D. W. Feldman, R. B. Feldman, W. J. D. Johnson, A. H. Lumpkin, R. L. Sheffield, R. W. Springer, W. E. Stein, and L. M. Young, "Performance of the Photoinjector Accelerator for the Los Alamos Free Electron Laser," published in *Proceedings of the 1991 IEEE Particle Accelerator Conference*, San Francisco, California, May 6–9, 1991 (IEEE Catalog No. 91CH3038-7), pp. 2754–2756.

23. K. Batchelor, H. Kirk, J. Sheehan, M. Woodle, and K. McDonald, "Development of a High Brightness Electron Gun for the Accelerator Test Facility at Brookhaven National Laboratory," published in *Proceedings of the 1988 European Particle Accelerator Conference*, Rome, Italy, June 7–11, 1988, edited by S. Tazzari (World Scientific, Singapore, 1989), pp. 954–957.

24. S. Heifets and S. Kheifets, "Optics of the NLCTA" (SLAC Advanced Accelerator Studies Note SLAC-AAS-70, April 1992).

25. S. A. Heifets and S. A. Kheifets, "Optics of a High-Gradient Linac" (SLAC Advanced Accelerator Studies Note SLAC-AAS-64, September 1991).

26. S. A. Heifets and S. A. Kheifets, "Longitudinal Electromagnetic Fields in an Aperiodic Structure" (SLAC-PUB-5907, September 1992), submitted to *IEEE Transactions on Microwave Theory and Techniques*; and "RF Pulse Transmission through an Accelerating Section" (SLAC Advanced Accelerator Studies Note SLAC-AAS-74, September 1992), to be published.